

SINTERING STUDIES ON Cu-Al-Ni POWDER MIXTURES

A THESIS SUBMITTED TO
THE GRADUATE SCHOOL OF NATURAL AND APPLIED SCIENCES
OF
THE MIDDLE EAST TECHNICAL UNIVERSITY

BY

CEREN BAĞDU

118917

**T.C. YÜKSEKÖĞRETİM KURULU
DOKÜMANTASYON MERKEZİ**

IN PARTIAL FULFILLMENT OF THE REQUIREMENTS FOR THE DEGREE OF
MASTER OF SCIENCE
IN
THE DEPARTMENT OF METALLURGICAL AND MATERIALS ENGINEERING

118917

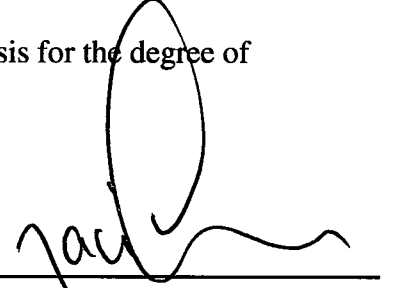
SEPTEMBER 2002

Approval of the Graduate School of Natural and Applied Sciences



Prof. Dr. Tayfur ÖZTÜRK
Director

I certify that this thesis satisfies all the requirements as a thesis for the degree of
Master of Science



Prof. Dr. Naci SEVİNÇ
Head of Department

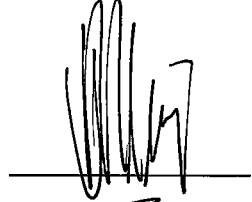
We certify that we have read this thesis and in our opinion it is fully adequate, in
scope and quality, as a thesis for the degree of Master of Science in Metallurgical and
Materials Engineering.



Prof. Dr. Bilgehan ÖGEL
Supervisor

Examining Committee Members:

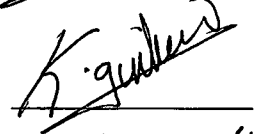
Prof. Dr. Vedat AKDENİZ



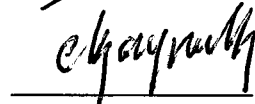
Prof. Dr. Bilgehan ÖGEL



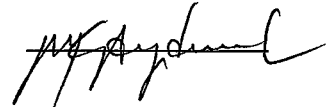
Assoc. Prof. Dr. Gürkan KARAKAŞ



Assoc. Prof. Dr. Cevdet KAYNAK



Assoc. Prof. Dr. Kadri AYDINOL



ABSTRACT

SINTERING STUDIES ON Cu-Al-Ni POWDER MIXTURES

BAĞDU, Ceren

M.S., Department of Metallurgical and Materials Engineering

Supervisor: Prof. Dr. Bilgehan ÖGEL

September 2002, 100 Pages

In this study, it is aimed to investigate sinterability of Cu-Al-Ni shape memory alloys produced from elemental Cu, Al and Ni powders. The powders were mixed to obtain a chemical composition of Cu-12^w/₀ Al-4^w/₀ Ni and were cold compacted and sintered at various pressures and temperatures.

Several sintering studies were carried out on the Cu-Al and Cu-Ni binary, and also on the Cu-Al-Ni ternary systems. As a result of these studies it was observed that the Cu-Al and Cu-Al-Ni specimens contained pores. So, these specimens could not be sintered to full density. This result showed that Al causes pore formation during sintering.

In order to investigate the reason of pore formation, several stepwise sintering and solid state sintering studies were carried out on the Cu-Al specimens, which were compacted at different pressures. As a result, it was found that the formation of liquid Al and its compositional solidification is not the only reason of pore formation. However, there are some other mechanisms taking place during solid state sintering of the compacts, which also contribute to pore formation.

Hot rolling operation was applied to Cu-Al, Cu-Ni and Cu-Al-Ni specimens after sintering. Cu-Ni specimens were successfully hot rolled, while surface cracks were observed in the hot rolled Cu-Al and Cu-Al-Ni specimens. The microstructural observations and EDS analysis of these specimens showed that, the residual Al_2O_3 inclusions originated from Al powder, is the main reason of the surface cracks. The residual Al_2O_3 inclusions could not be reduced under conventional sintering atmospheres.

Key Words: Cu-Al-Ni Shape Memory Alloys, Powder Metallurgy, Sintering, Pore Formation.

ÖZ

Cu-Al-Ni TOZ KARIŞIMLARININ SİNERLEME ÇALIŞMALARI

BAĞDU, Ceren

Yüksek Lisans, Metalurji ve Malzeme Mühendisliği Bölümü

Tez Yöneticisi: Prof. Dr. Bilgehan ÖGEL

Eylül 2002, 100 sayfa

Bu çalışmada, saf Cu, Al ve Ni tozları ile üretilen Cu-Al-Ni şekil bellek alaşımının sinterlenebilirliğinin incelenmesi amaçlanmıştır. Bu tozlar, Cu-12 % Al-4 % Ni kimyasal kompozisyonunu elde etmek üzere karıştırılmış ve değişik basınçlarda soğuk preslenmiş ve çeşitli sıcaklıklarda sinterlenmiştir.

Cu-Al ve Cu-Ni ikili sistemleri ve Cu-Al-Ni üçlü sistemi üzerinde çeşitli sinterleme çalışmaları yapılmıştır. Bu çalışmaların sonunda, Cu-Al ve Cu-Al-Ni numunelerinin gözenek içerdiği gözlenmiştir. Sonuç olarak, bu numunelerin sinterlemesi sonunda gözenekler tam olarak yok edilememiştir. Bu sonuç, alüminyum tozunun sinterleme sırasında gözenek oluşuma neden olduğunu göstermiştir.

Gözenek oluşumunun nedenini incelemek amacıyla, farklı basınçlarda preslenmiş Cu-Al numuneleri üzerinde birtakım basamaklı sinterleme ve katı hal sinterleme çalışmaları yapılmıştır. Sonuç olarak, gözenek oluşumunun tek nedeninin alüminyumun sıvılaşması ve bunun kimyasal bileşime bağlı katılaşması olmadığı ortaya çıkarılmıştır. Bunun yanında, gözenek oluşumuna ayrıca katkıda bulunan ve numunelerin katı hal sinterlemesi sırasında yer alan başka birtakım mekanizmalar olabileceği sonucuna varılmıştır.

Bunlara ek olarak, sinterlenmiş Cu-Al, Cu-Ni ve Cu-Al-Ni numuneleri sıcak haddelenmiştir. Cu-Ni numuneleri başarıyla haddelenebilirken, sıcak haddelenmiş Cu-Al ve Cu-Al-Ni numunelerinde yüzey çatlakları gözlenmiştir. Bu numunelerin mikroyapısal ve E.D.S. nokta analizleri, Al tozundan gelen Al_2O_3 kalıntılarının yüzey çatlağı oluşumunun esas nedeni olduğunu göstermiştir. Kalıntı Al_2O_3 laboratuvar koşullarında indirgenememiştir.

Anahtar Kelimeler: Şekil Bellekli Cu-Al-Ni Alaşımları, Toz Metalurjisi, Sinterleme, Gözenek Oluşumu.

To
Sami, Seçkin and Duygu BAĞDU

ACKNOWLEDGEMENTS

I would like to express my special appreciation to my supervisor Prof. Dr. Bilgehan ÖGEL for his great guidance, supervision and encouragement throughout the study.

I am very grateful to all my friends who supported me during the hard times. Special thanks to Benat Bilçen Koçkar, Cansu Gürhan, Ziya Esen, Cem Denk and to my family, for their help, guidance, patience and encouragement during the entire period of my study.

Finally, thanks to all the technical staff of the Metallurgical and Materials Engineering Department for their suggestions and assistance during this study.

TABLE OF CONTENTS

ABSTRACT	iii
ÖZ.....	v
DEDICATION	vii
ACKNOWLEDGEMENTS	viii
TABLE OF CONTENTS	ix
CHAPTER	
1 INTRODUCTION.....	1
2 THEORY.....	3
2.1 Shape Memory Behavior.....	3
2.2 Cu-Based Shape Memory Alloys.....	8
2.3 Production of Shape Memory Alloys	10
2.4 Powder Metallurgy	12
2.4.1 Fabrication of Metal Powders.....	12
2.4.2 Powder Characterization.....	14
2.4.3 Precompaction Powder Handling.....	14
2.4.4 Powder Compaction	15
2.4.5 Sintering	18

2.4.6	Liquid Phase Sintering.....	24
2.4.6.1	Transient Liquid Phase Sintering	27
2.4.6.2	Pore Formation and Swelling During Liquid Phase Sintering	29
2.5	Powder Metallurgy of Cu-Based Alloys	31
2.6	Powder Metallurgy of Cu-Based Shape Memory Alloys.....	35
3	EXPERIMENTAL PROCEDURE.....	37
3.1	Material Used	37
3.2	Experimental Set-up and Technique.....	37
3.2.1	Mixing	37
3.2.2	Cold Compaction.....	38
3.2.3	Sintering	38
3.2.4	Hot Rolling.....	38
3.3	Investigated Systems	39
3.4	Density Measurement.....	43
3.5	Metallographic Examination	46
4	EXPERIMENTAL RESULTS	47
4.1	Sintering Studies on Cu-Al System.....	47
4.2	Sintering Studies on Cu-Ni System.....	62
4.3	Sintering Studies on Cu-Al-Ni System.....	70
4.4	Hot Rolling Studies on Cu-Al, Cu-Ni and Cu-Al-Ni Systems.....	73
4.5	Grain Refining Studies	80

5	DISCUSSION.....	84
5.1	Pore Formation in Cu-al System	85
5.2	Hot Rolling Studies	88
5.3	Effect of Compaction Pressure and Sintering Route on the Final Density	91
6	CONCLUSION	95
	REFERENCES	97



CHAPTER 1

INTRODUCTION

Shape memory alloys have been extensively studied since 1951, when the first shape memory alloy (Au-Cd) was found by Chang and Read [1]. Since their discovery, they have been very popular in the technological world due to their shape memory effect and superelasticity for many different applications. The alloy systems that reveal shape memory behavior can be listed as: Ti-Ni, Au-Cd, In-Tl and Cu-based alloys. Among these, only Ti-Ni and Cu-based alloys have been successfully applied in various industrial projects and laboratory adventures [2]. Ti-Ni based shape memory alloys exhibit good properties in strength, ductility and resistance to corrosion, which are important for practical use. However, they are very expensive, compared with Cu-Based shape memory alloys. Hence, inexpensive Cu-based shape memory alloys have been investigated and developed, which have advantages in electrical and thermal conductivities and deformability, compared with Ti-Ni based shape memory alloys [3]. Cu-Al-Ni alloys are better shape memory alloys in terms of their thermal stability and corrosion resistance [4].

The shape memory alloys are usually produced by induction melting and casting, and shaped by conventional methods such as rolling and wire drawing. However, the conventional casting method has difficulties in controlling the grain size and alloy composition and homogeneity. Coarse grains will weaken the mechanical

properties and increase the transformation temperatures. Uncontrolled composition will make transformation temperatures unpredictable. To eliminate these problems, some alternative production methods i.e. Powder Metallurgy, have been developed to obtain shape memory alloys with fine grains and to control the alloy composition.

Several studies were carried out about the production of several shape memory alloys by powder metallurgical techniques. Lu et al. [5] investigated the production of Cu-Zn-Al shape memory alloys by powder metallurgical methods. The prealloyed powders were mechanically alloyed under Argon atmosphere to reduce oxidation. Jean et al. [6], Tang et al. [7] and Duerig et al. [8] have studied on the production of Cu-Al-Ni shape memory alloys starting from pre-alloyed powders. In the study of Jean et al., the prealloyed powders were hot pressed and sintered. However, Tang et al. and Duerig et al. applied cold compaction to consolidate the prealloyed powders. The reason of using prealloyed powders in these studies was to obtain a homogenous material with shorter sintering times.

The aim of the present study is, to produce Cu-Al-Ni shape memory alloys by powder metallurgical techniques, starting from elemental Cu-Al- and Ni powders. The conventional powder metallurgical route of cold compaction followed by a sintering process was applied to the powder mixtures. To obtain the optimum production parameters, several sintering and densification studies were carried out throughout the study. For this purpose the Cu-Al and Cu-Ni binary systems were investigated first. The two main parameters were the compaction pressure and sintering route. Then, the study focused on the reason of pore formation in Cu-Al system, which is also causes porosity in the Cu-Al-Ni system. The obtained results were used to produce Cu-Al-Ni system with highest density. Finally hot rolling was applied to the sintered specimens of Cu-Al, Cu-Ni and Cu-Al-Ni systems.

CHAPTER 2

THEORY

2.1. SHAPE MEMORY BEHAVIOR

Shape memory refers to the ability of certain materials to remember a shape, even after rather severe deformations: once deformed at low temperatures (in their martensitic phase), these materials will stay deformed until heated, whereupon they will spontaneously return to their original, pre-deformation shape [4]. Materials that exhibit shape memory only upon heating are referred to as having *one-way shape memory*. Some materials also undergo a change in shape upon recooling. These materials have two-way shape memory. A shape memory alloy may be further defined as one that yields a thermoelastic martensite. In this case, the alloy undergoes a martensitic transformation of a type that allows the alloy to be deformed by a twinning mechanism below the transformation temperature. The deformation is then reversed when the twinned structure reverts upon heating to the parent phase [9].

In order to understand the elementary engineering aspects of the shape memory first, we should become familiar with some basic principles of martensite and its formation.

Martensite transformation can be defined simply as a lattice transformation involving shearing deformation and resulting from cooperative atomic movement. The atoms within the lens- or plate-shaped areas in the parent phase are not shifted independently but undergo shearing deformation as a unit while maintaining a domino-like coordination until the parent lattice transform into martensite. With this kind of cooperative movement of atoms, a 1-to-1 correspondence, called ‘lattice correspondence’, persists between the lattice points in the parent phase and the points in the martensite phase [10].

The properties listed below follow from the definition of martensitic transformations:

- 1) The martensite phase is a substitutional or interstitial solid solution.
- 2) The transformation is diffusionless. The concentration of solute atoms dissolved in the martensite phase is equal to that in the parent phase. There is no long-distance diffusion such as occurs in eutectoid transformations.
- 3) The transformation is accompanied by shape changes (or surface relief) of a definite value.
- 4) A martensite crystal has a specific ‘habit plane’. This is the plane along which shear occurs during the transformation.
- 5) There is a definite orientation relationship between the parent and martensite phase lattices.
- 6) On a macroscopic scale the shape strain in martensite is an ‘invariant plane strain’. The strain that produces a homogenous deformation with an invariant habit plane is called an *invariant plane strain*. In this type of strain the displacement of any point is a linear function of the distance of that point from the invariant plane. The martensitic transformations involve a simple shear combined with a uniaxial tension or compression normal to the habit plane [11].

Thermoelastic martensites are characterized by their low energy and glissile interfaces, which can be driven by small temperature or stress changes. The transformation, although a first-order phase change, does not occur at a single temperature but over a range of temperatures that varies with each alloy system [2]. In thermoelastic martensitic transformations the so-called hysteresis which is the difference between the austenite start and martensite start temperatures (A_s - M_s) is extremely small compared to the non-thermoelastic martensitic transformations (Figure 2.1). This indicates that the driving force required in the austenite to martensite transformation to overcome the transformation strain energy is very low [12].

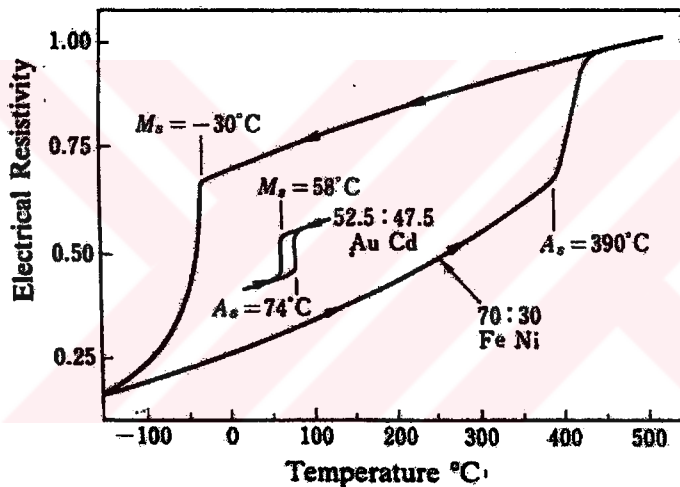


Figure 2.1 Comparison of the Temperature Hysteresis in Non-Thermoelastic (FeNi) and Thermoelastic (AuCd) Martensitic Transformations [12]

In order for the shape recovery to be complete, deformation by slip must not be involved in the deformation process, since deformation by slip is an irreversible process. The main mode of deformation in SMAs in a complete martensitic state can be said to be essentially a twinning deformation [10]. If the crystal structure change was accompanied by slip rather than by twinning, the elastic strain limit of the material would be exceeded, the mobile low energy boundaries of the

martensite would be locked by the dislocations, and as a result unrecoverable plastic deformation would be introduced into the structure [13].

As described above, in order for thermoelastic martensitic transformations to occur, both the interface energy and energy needed by the plastic deformation must be so small that they can be neglected. This is possible when during the transformation the structure changes and, consequently, the volume changes are both small, and when there is good coherency between the parent phase lattice and the martensite phase lattice. Generally, these conditions are satisfied if the parent phase has an ordered structure. The reason most thermoelastic transformations occur in ordered alloys is that the crystallographic reversibility, which characterizes the transformation, is automatically guaranteed by superlattice structures [10].

The mechanical properties of shape memory alloys vary greatly over the temperature range spanning their transformation. Normally, on cooling the martensite forms at M_s under no stress. But in the same material, martensite can form above M_s if as stress is applied, and the martensite so-formed is termed stress-induced martensite. This is called pseudoelasticity and with this property martensite can be made stable with the application of stress, but becomes unstable again when the stress is removed [4].

In most cases, the memory effect is one-way. That is, upon cooling, a shape memory alloy does not undergo any shape change, even though the structure changes to martensite. When the martensite is strained up to several percent, however, that strain is retained until the material is heated, at which time shape recovery occurs [9].

It is possible in some of the shape memory alloys to cause two-way shape memory. That is, shape change occurs upon both heating and cooling. The amount of this shape change is always significantly less than obtained with one-way

memory, and very little stress can be exerted by the alloy as it tries to assume its low-temperature shape. A number of heat-treatment and mechanical training methods have been proposed to create the two-way shape memory effect. All rely on the introduction of microstructural stress concentrations which cause the martensite plates to initiate particular directions when they form upon cooling, resulting in an overall net shape change in the desired direction [9].

Alloys having a shape memory effect can be listed as:

Ag-Cd , Au-Cd, Cu-Al-Ni, Cu-Sn, Cu-Zn, Cu-Zn-X (X = Si,Sn,Al), In-Ti, Ni-Al, Ni-Ti, Fe-Pt, Mn-Cu, Fe-Mn-Si.

Among these alloys, both Ni-Ti and Cu-based shape memory alloys, such as Cu-Zn-Al and Cu-Al-Ni are presently available for commercial shape memory applications. The NiTi alloys have greater shape memory strain (up to 8% versus 4 to 5% for the copper-base alloys), tend to be much more thermally stable, have excellent corrosion resistance compared to the copper-base alloys' medium corrosion resistance and susceptibility to stress-corrosion cracking [9]. However NiTi in finished form is very expensive because of fabrication difficulties associated with melting and forming.

In many applications, Cu-based alloys provide a more economical alternative to Ni-Ti [4]. Copper base alloys can be melted and extruded in air with ease, and have wider range of potential transformation temperatures [9]. Although early Cu-based alloys suffered from intergranular failure due to their intrinsic coarse grain structure, the recent development of fine-grain Cu-based memory alloys are more competitive than Ni-Ti when comparing to bimetals and other low cost materials commonly used in conventional thermal-mechanical actuation mechanisms [4].

2.2. Cu-BASED SHAPE MEMORY ALLOYS

Current Cu-based shape memory alloys are derived from three binary alloy systems: Cu-Zn, Cu-Al and Cu-Sn as can be seen in Figure 2.2. The martensitic transformation in Cu-Sn alloy is not ideally thermoelastic and suffers from a rapid degradation of shape memory properties during aging at even moderate temperatures. These alloys therefore have been more of a laboratory interest in aging studies than as potential commercial shape memory alloys [4].

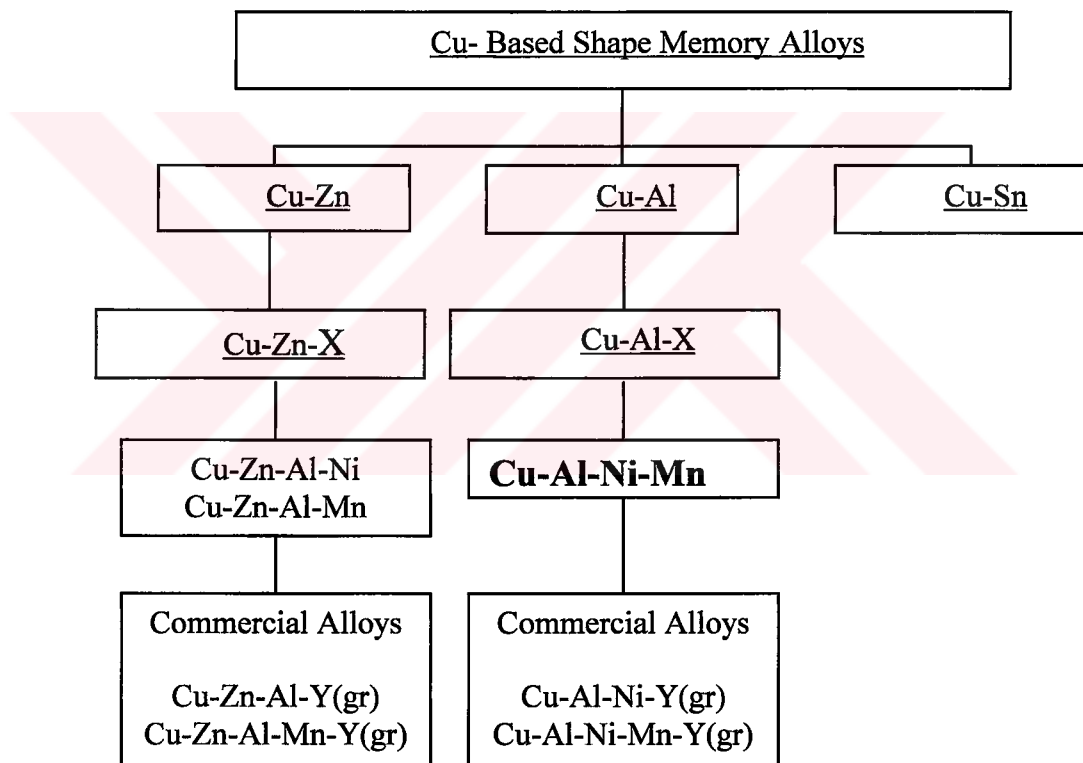


Figure 2.2 Classification of Cu-based shape memory alloy systems and their alloying elements [4]

On the contrary, alloys that are formed with several element additions to the Cu-Zn and Cu-Al binary systems show useful shape memory properties. Among the ternary systems, especially Cu-Zn-Al [14] and Cu-Al-Ni [8,15] have been studied because of their good shape memory properties. The studies have also been

extended to quaternary alloys of Cu-Zn-Al-Ni [16], Cu-Zn-Al-Mn [17] and Cu-Al-Ni-Mn [18]. Both the ternary alloys Cu-Zn-Al and Cu-Al-Ni, and quaternary modifications containing Mn have been developed as commercially available alloys.

If the most widely used two main groups of Cu-based shape memory alloys, namely Cu-Zn and Cu-Al are compared; the Cu-Al-Ni alloys are better shape memory alloys in terms of their thermal stability and corrosion resistance. However, their one disadvantage is the higher processing costs because of their lack of appropriate low temperature ductility [4]. Generally, Ni, Be, Zn, Mn is added to Cu-Al binary system in order to have shape memory alloys. The aim of adding a third or fourth element is to adjust the transformation temperature and grain refining.

In fact, for all the shape memory alloys the control and adjustment of the transformation temperature is extremely important. In the Cu-Al-Ni system transformation temperature is affected by three factors: composition, grain size and quenching rate.

Composition: the martensitic transformation temperature is very sensitive to small variations in alloy composition. To a first approximation, the transformation temperature follows a linear relationship with alloying element content.

Cu-Zn-Al

$$A_s(^{\circ}\text{C}) = 2117 - 58,79(\text{wt}\%\text{Zn}) - 149,64(\text{wt}\%\text{Al})$$

$$M_s(^{\circ}\text{C}) = 2212 - 66,9[1,355(\text{at}\%\text{Al}) + 1(\text{at}\%\text{Zn})]$$

Cu-Al-Ni

$$M_s(^{\circ}\text{C}) = 2020 - 45(\text{wt}\%\text{Ni}) - 134(\text{wt}\%\text{Al})$$

The presence of Ni in Cu-Al-Ni alloys shifts the Cu-Al eutectoid to higher Al content and retards the hypereutectoid decomposition. Ni contents up to 4% also help to reduce the transformation hysteresis. Commercially, quaternary Cu-base shape memory alloys also contain Mn. Mn also shifts the Cu-Al eutectoid to higher Al content.

Grain size: Because of rapid grain growth, heat treated Cu-base shape memory alloys usually possess coarse grains with sizes in the mm range. Coarse-grained Cu-base alloys are brittle and prone to premature intergranular failure. They also exhibit shorter thermomechanical cycling life due to rapid degradation in shape memory performance.

Among the grain refining elements listed in Figure 2.2, B, Ti and Zr are very effective in refining the grain structure. Grain refining elements usually have very limited solubility in Cu-base shape memory alloys. Refining is largely due to the formation of small insoluble particles, which either assist grain nucleation or inhibit grain growth.

2.3. PRODUCTION OF Cu-BASED SHAPE MEMORY ALLOYS

The two parameters of transformation temperature for shape memory alloys; composition and grain size of the alloy are primarily determined by the production technique. In the following section two basic production techniques will be introduced.

Casting

Shape memory alloys are usually produced by induction melting and shaped by conventional methods such as rolling and wire drawing. [19]. One special technique used for the production of Cu-Al-Ni shape memory alloys is Twin Roll Casting, which provides the production of thin foils with a cooling rate of 104-105 K/s.

Powder Metallurgy and Rapid Solidification

Fine grain Cu-base shape memory alloys without grain-refining element additions can be produced by powder metallurgy or rapid solidification processing. A grain size of around 30 μm has been obtained in a powder processed Cu-Zn-Al alloy [20]. Which was water atomized to an averaged particle size of 150 μm and subsequently cold compacted and hot extruded. Powder processed Cu-Zn-Al shows better resistance to cycling degradation in recoverable strain than cast alloys [4]. A powder processed Cu-Al-Ni alloy with grain size of 20 μm also exhibits a significantly improved ductility (5 to 7% compared to 0,6% in cast alloys) [8].

Fine grain Cu-base shape memory alloys with grain sizes of 1-20 μm have also been obtained by rapid solidification processing techniques, such as melt spinning [21, 22] and melt extraction [23]. Because of their small grain size and large quenched-in defect population, rapidly solidified Cu-Zn-Al [24] and Cu-Al-Ni [22] alloys show transformation at lower temperatures than nominal.

As a result, Cu-based shape memory alloys can be produced via conventional casting or powder metallurgy methods. But, due to some problems resulting from casting, which are previously discussed, powder metallurgy techniques are being studied more and more each day.

2.4. POWDER METALLURGY

Among the various metalworking technologies, powder metallurgy is the most diverse manufacturing approach. One attraction to powder metallurgy (P/M) is its ability to fabricate high quality, complex parts to close tolerances in an economical manner. The process effectively uses automated operations with low energy consumption, high material utilization and low capital costs. These characteristics make P/M well aligned with current concerns about productivity, energy and raw materials. Consequently the field is experiencing growth at the expense of alternative metalforming operations [25].

A powder is defined as a finely divided solid, smaller than 1 mm in its maximum dimension. Another important characteristic of a powder is its relatively high surface area to volume ratio. Powder Metallurgy is the study of the processing of metal powders, including the fabrication, characterization and conversion of metal powders into useful engineering components [25].

There are three main steps to the scheme of powder metallurgy. First is the powder technology. In this area emphasis is given to fabrication, classification, characterization and handling of powders. Secondary concerns are with the sampling, safety, packaging and transportation. Next come the traditional powder metallurgy activities such as compaction and sintering. The concerns at this stage are with the shaping, forming and densification of the powders. Finally, the conceptual flow turns to an emphasis on the properties, with primary attention to microstructure.

2.4.1. Fabrication of Metal Powders

A basic understanding of powder characteristics relies on knowledge of powder fabrication. Knowledge of the powder fabrication technique provides a good basis for estimating the powder characteristics. The method selected for fabricating a

powder depends on specific properties of the material. The four main categories of fabrication techniques are mechanical, chemical, electrolytic and atomization.

1-Mechanical Fabrication Techniques: there are three main techniques for the mechanical fabrication. These are;

- a) **Machining:** coarse powder with an irregular shape results from the shear associated with the machining of wrought metal.
- b) **Milling:** milling by mechanical impaction using hard balls is a classical approach to fabricating powders from brittle materials. Milling is not useful for most metals because of their ductility, cold welding and low process efficiency.
- c) **Mechanical Alloying:** mechanical alloying employs the attrition motion between agitated balls to create a microalloyed composite powder. On a macroscopic scale, the repeated milling, cold-welding and fracture of metal powder.

2-Electrolytic Fabrication Techniques: a powder can be precipitated at the cathode of an electrolytic cell under certain operating conditions. Common examples of metals formed by this method include titanium, palladium, copper, iron, and beryllium. The main attraction of an electrolytic approach is the high product purity.

3-Chemical Fabrication Techniques: almost all metals can be fabricated into powder by a chemical technique. There are several variants to the chemical synthesis approach; powders can be formed by gas-solid, liquid, or vapor phase reactions.

4- Atomization Fabrication Techniques: Atomization involves the formation of powder from molten metal using a spray of droplets [25]. The basic procedure most often employed is to force a liquid metal through an orifice, and impinge a

gas or liquid (mostly water) stream on the emerging melt [26]. Both elemental and prealloyed powders can be formed by such processes.

2.4.2. Powder Characterization

Powder characteristics have a great influence on processing and the final properties. For powder characterization, the seven quantitative data are required:

1) Particle size and its distribution, 2) particle shape and its variation with particle size, 3) surface area, 4) interparticle friction, 5) flow and packing, 6) the internal particle structure, 7) Chemical gradients, surface films and admixed materials [25].

The apparent density of a powder refers to the weight of a unit volume of loose powder. This quantity strongly affects the green density and consequently, final density of the powder compact. The apparent density decrease with decreasing particle size, with the departure of particle shape from sphericity, and with increasing surface roughness. Additionally, the apparent density can be manipulated by mixing various sizes of particles (a broad particle distribution) [26].

There are several techniques used to characterize the powder. Most important ones are; microscopy, screening, sedimentation, light screening, electrical conductivity, light blocking and X-Ray techniques.

2.4.3. Precompaction Powder Handling

It is necessary to tailor specific properties into a powder for easier compaction and sintering. Examples of operations that occur in the precompaction stage include classification, blending, mixing, agglomeration, deagglomeration, and lubrication.

Classification is used to obtain a specific size fraction from a powder. Blending and mixing both combine powders into a homogenous mass. Blending refers to the

combination of different sized powders of the same chemistry, while mixing implies different powder chemistries. Attrition and deagglomeration are useful in those instances when a fine, discrete powder is needed. Alternatively, fine powders, which exhibit a high interparticle friction and do not flow, can be agglomerated into coarser particles. Finally, lubrication of a powder using organic molecules provides for easier part ejection from compaction tooling and longer die life.

Mixing and blending are the two most common precompaction steps. Powders are blended to achieve control over the particle size distribution. Powders can be mixed to form new compositions. The mechanisms of powder mixing are diffusion, convection and shear. A diffusional mix occurs by the motion of individual particles into the powder lot. Convective mixing refers to a transfer of adjacent powder groups from one location to another. Shear mixing occurs by continual division and flow of the powder over slip planes [25].

2.4.4. Powder Compaction

In most applications for powder metallurgy, concern with properties dictates that high densities be achieved in compaction.

The compaction of powders has the following major functions: [26]

- 1) To consolidate the powder into the desired shape
- 2) To impart, to as high a degree as possible, the desired final dimensions with due consideration to any dimensional changes resulting from sintering;
- 3) To impart the desired level and type of porosity;
- 4) To impart adequate strength for subsequent handling.

At the beginning of a compaction cycle, the powder has a density approximately equal to the apparent density. As pressure is applied, the first response is rearrangement of particles, giving a higher packing coordination. Initially, the

number of particle contacts grows as particle rearrangement and sliding occurs. High pressures increase density by contact enlargement through plastic deformation. Thus, the pressure causes localized deformation at the contacts, giving work hardening and allowing new contacts to form as distance between particles decreases.

During deformation, cold welding at the interparticle contacts contributes to the development of strength in the compact. As the compaction pressure is further increased, the amount of each particle undergoing plastic deformation increases and homogenous plastic flow occurs throughout the compact. With considerable work hardening or with brittle materials, densification can occur by fragmentation. The compact surface area increases because of fragmentation; however, the strength shows little improvement.

At very high compaction pressures, in excess of 1 GPa, massive deformation occurs, leaving fine pore sizes. Continual pressurization beyond this level is of little benefit. Relief of the pressure results in relaxation of the material with an elastic springback, which is the main cause of delamination.

An understanding of two important parametric relations is necessary in a discussion of compaction. The first is the dependence of the green density on the compaction pressure.

Second, is the variation of green properties with either density or compaction pressure. As the pressure is increased, the compact density increases, or alternatively, the porosity decreases. But, in die pressed compacts, density gradients result from the pressure gradients. Here, the height to diameter ratio (H/D) is very important. As the H/D ratio is increased, density gradients will increase and the overall compact density will decrease. It can be seen from Figure 2.3 that, as the H/D ratio is increased, the density gradients in the compact increase and the bulk density decreases.

The type of pressure application, namely whether the pressure is applied with a single or double ended pressing, also determines the density gradients in the compact. The effect of this factor can be seen in Figure 2.4. In single ended pressing, the density is highest at the top of the compact and decreases towards the bottom. However, in double-ended pressing the minimum density is achieved at the center of the compact, but the density distribution is more homogenous than that of the single ended pressing.

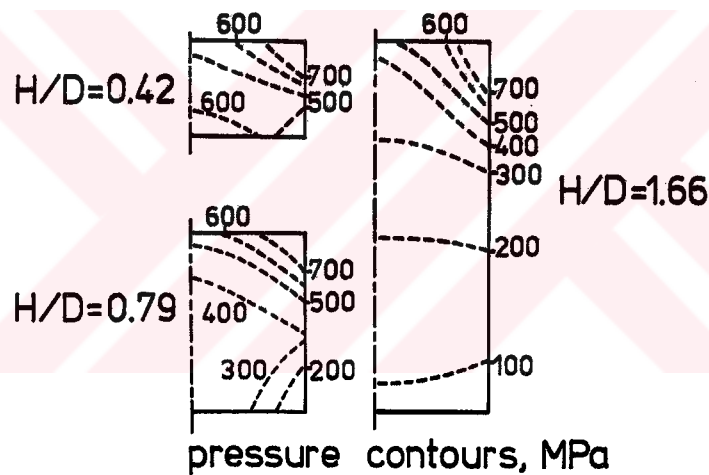


Figure 2.3 Pressure distribution in cylindrical copper powder compact of three H/d ratios [25]

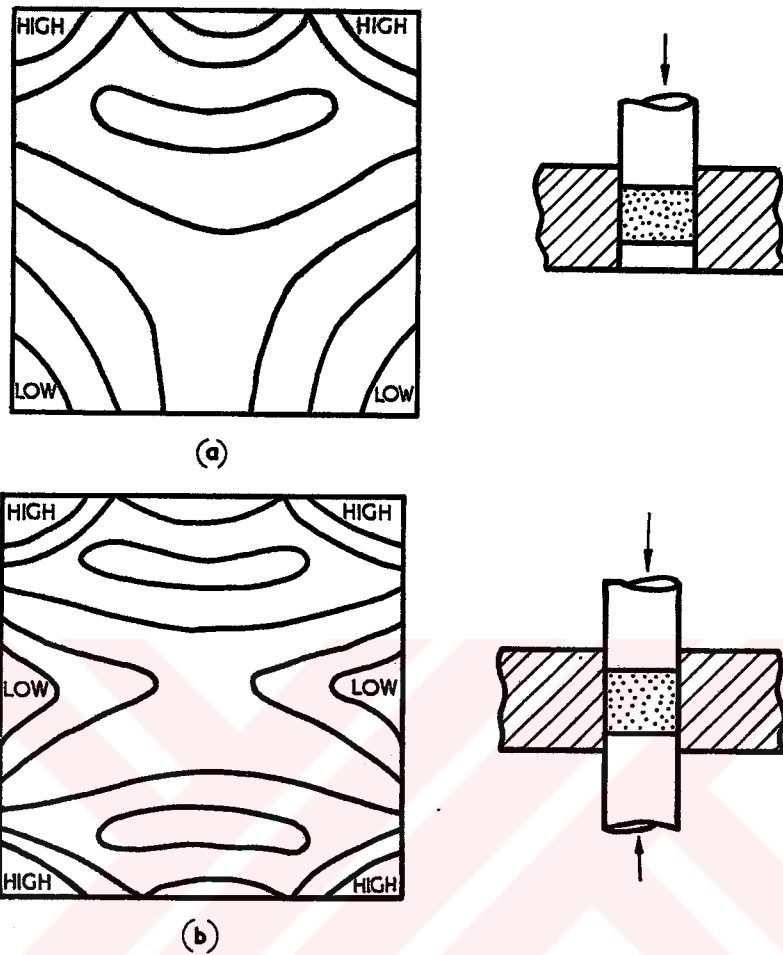


Figure 2.4 Density distribution in single-ended and double-ended pressing [27]

2.4.5. Sintering

Loose powders can be cold shaped as mentioned previously. However, the shaped body will be very fragile, and it cannot withstand even small-applied stresses due to the insufficient degree of interparticle bonding. Therefore, it is necessary to strengthen the bonding between particles to produce a structure, which can withstand high stress. For this purpose, the fundamental process of powder metallurgy; i.e. sintering, is applied to cold shaped bodies. *Sintering* is a thermal treatment for bonding particles into a coherent, predominantly solid structure via

mass transport events that often occur on the atomic scale. The bonding leads to improved strength and a lower system energy.

To talk about sintering, we need to have measures for the process. Among a wide array of measurements, a few selected observations prove most valuable. These might include a combination of surface area, neck size, shrinkage, porosity, or density. Measurements made as a function of sintering time or sintering temperature allow examination of the sintering kinetics.

Compaction Effects on Sintering

Pressure forms loose particles into shapes with prescribed dimensions and a better packing density than that of loose powder. The compaction processes involves particle rearrangement, deformation, and possibly fracture. With compaction, there is a reduction in the pore size and porosity, while there is an increase in the dislocation density in the powder. Because of the lower porosity, there is less shrinkage during sintering. The higher dislocation density contributes to an initially faster sintering rate. Compaction therefore contributes to increased strength, density, shape definition and dimensional control.

The higher compaction pressures contribute to an increase in density and neck contact size, while reducing the rate of neck growth during sintering. Also, shrinkage decreases with an increasing compaction pressure. It is the sintered neck size, which dominates the properties such as strength and ductility. Thus, higher compaction pressure gives better dimensional control, less sintering shrinkage, and better final properties.

Density, Porosity, and Pore Characteristics

Density is the most widely reported property in sintering. Unlike the absolute density (Mg/m^3 or g/cm^3), which depends on composition, the fractional or percentage density gives evidence of the fundamental events occurring during sintering, independent of the material. It is defined as the measured density divided by the theoretical density.

Pores are an inherent part of sintering. They are present in the powder compact as interparticle voids. Also, during sintering pores can form from uneven phase distribution, unbalanced diffusion events, reactions with the atmosphere, and capillary spreading of a liquid upon melting. Porosity, gives the fraction of the total volume that is void. It is expressed as either a percentage or fraction of the total volume. Pore size, shape and connectivity are typical concerns during sintering. The measurement of these attributes is possible by several techniques. Optical and electron microscopy are usually most suitable. The other techniques include, mercury porosimetry, impregnating fluids or epoxy resins.

Shrinkage and Swelling

Formally, the linear dimension change is defined as $\Delta L/L_0$, reflecting the change in an initial green length L_0 to a final sintered length L_s given as ΔL . If the dimension is larger after sintering, the process is termed swelling and $\Delta L/L_0$ is positive, while if the dimension is smaller after sintering the process is termed shrinking and $\Delta L/L_0$ is negative. The higher the sintering temperature, the longer the sintering time, the finer the particle size of powder, and the lower the green density of the compacts, the greater the shrinkage. Expansion during sintering is common in compacts made of soft metal powders, such as copper, that are pressed at high pressures [28]. This expansion is due to gases entrapped in closed-off pores of the compact [29].

Surface Area

During sintering, there is a progressive loss of surface area. Even if a powder fails to shrink during sintering, the growth of interparticle bonds will reduce the surface area. In the early portion of sintering, there is a good correlation between neck size ratio (X/D), and the loss of surface area $\Delta S/S_0$:

$\Delta S/S_0 = -k_s(X/D)^M$ where $\Delta S/S_0$ is the change in surface area divided by the original, unsintered surface area and M is the exponent typically in the range 1,8 to 2 and depends on the transport mechanism and initial compact density.

The principle driving forces for sintering are capillary forces due to surface and interfacial tensions, also called specific surface and specific interfacial free energies, of the free surfaces and the interfaces between grains [30]. Stresses due to surface and interfacial tension forces tend to decrease the surface and the interfacial areas and are the principle driving forces in sintering [29].

There are several mass transport paths in sintering. The two main categories are surface transport and bulk transport as it is also shown in Figure 2.5. It is the latter that is responsible for densification during sintering. Evaporation-condensation and surface diffusion are the common surface transport processes.

Materials with high vapor pressures or those that form a volatile species by reacting with the sintering atmosphere are the candidates for **evaporation-condensation** controlled sintering. Evaporation occurs from a surface and transport occurs across pore space, leading to condensation on a nearby surface. The net result over time is a reduction in the total surface area as bonds grow between touching particles, but there is no change in the distance between particle centers. **Surface diffusion** also produces a loss of surface area during neck growth but fails to induce shrinkage or densification. Surface diffusion becomes an active process during heating to the sintering temperature. It initiates at lower

temperatures in comparison with other sintering mechanisms. It involves mass flow from surface sources to surface sinks and does not produce any shrinkage.

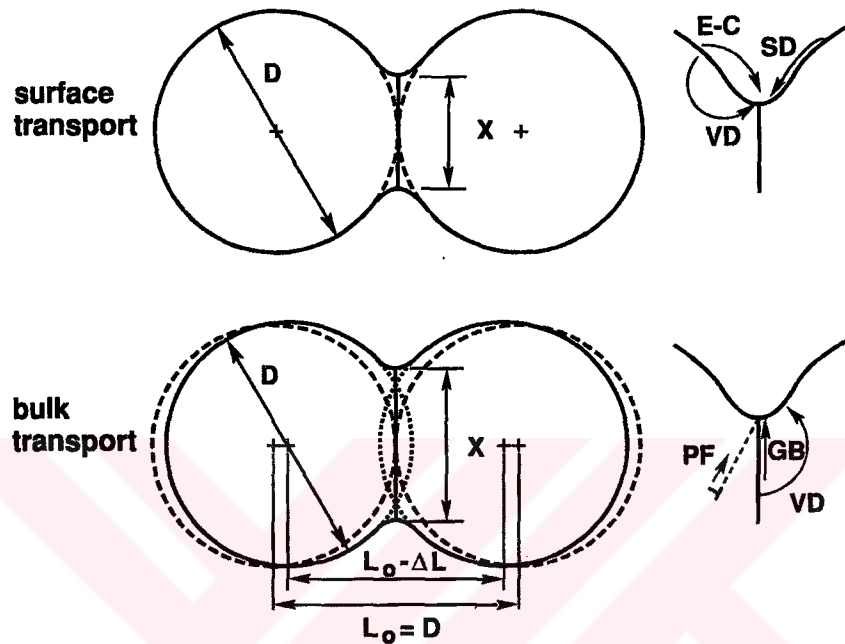


Figure 2. 5 Two classes of mass transport mechanisms during sintering applied to the two-sphere model (E-C; Evaporation-Condensation, SD; Surface Diffusion, VD; Volume Diffusion, PF; Plastic Flow, GB; Grain Boundary Diffusion) [31]

Crystalline materials densify during sintering by **bulk transport processes** of grain boundary diffusion, volume diffusion, and plastic flow. Grain boundaries form in the sinter bond between individual particles due to misaligned crystals. This defective character of the grain boundary allows mass flow with an activation energy that is usually intermediate between that for surface diffusion and volume diffusion. Mass is removed along the grain boundary and redeposited at the sinter bond. The interparticle grain boundaries, and internal grain boundaries in the particles, acts as vacancy annihilation sites by process of slip and rotation. The mass flows along the grain boundary, to be deposited at the bond between

particles. **Volume diffusion**, or lattice diffusion, involves the motion of vacancies through a crystalline structure. Due to vacancy concentration potentials (differences) in the solid, vacancies move from regions of high concentrations to regions of lower ones. The atoms then move in the opposite directions, leading to densification. **Plastic flow** is favored during heating to the sintering temperature and involves both dislocation climb (via vacancy annihilation) and possibly dislocation glide. Dislocations interact with vacancies during sintering to improve mass transport. The dislocation climb by the absorption of vacancies emitted from the pores, leading to annihilation of the vacancies and dislocation motion to a new slip plane.

Consider two spherical particles in contact such as shown in Figure 2.6. As the bond between the particles grows, the microstructure changes as shown in Figure 2.7. The initial stage of sintering is defined as occurring while the neck size ratio (X/R) is less than 0.3 for uncompact powders. During this stage, the kinetics is dominated by the sharp curvature gradients located near the interparticle neck. The pore structure is open and fully interconnected, although the pore shape is not very smooth. Analysis of the driving force for initial stage sintering shows that it is the curvature gradient at the neck, which guides the mass flow.

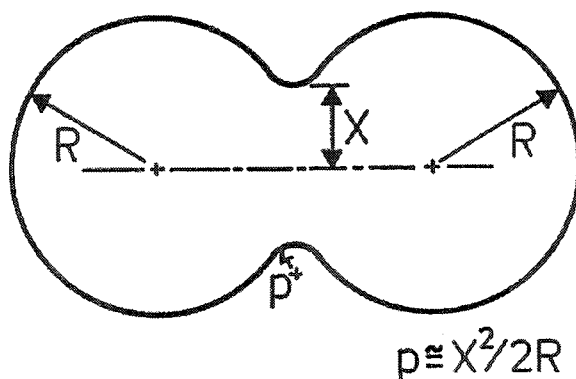


Figure 2.6 The sintering profile for two spherical particles with a neck radius of X . The sphere radii are R and the circular profile of the neck has a radius of p [25]

In the intermediate stage, the pores have an interconnected, cylindrical structure. The predominant development of compact properties occurs in the intermediate stage. The driving force is the interfacial energy. Densification is accomplished by volume and grain boundary diffusion. During the intermediate stage the pore structure is open and interconnected. The final stage of sintering occurs when the pores spheroidize into a closed structure. Neck growth continues in the intermediate stage; however, the neck shape is lost as the pores become smooth. In the final stage, kinetics is very slow. The driving force is the elimination of pore-solid interfacial area. The isolated spherical pores shrink with bulk diffusion. The presence of a gas in the pore will limit the amount of final stage densification.

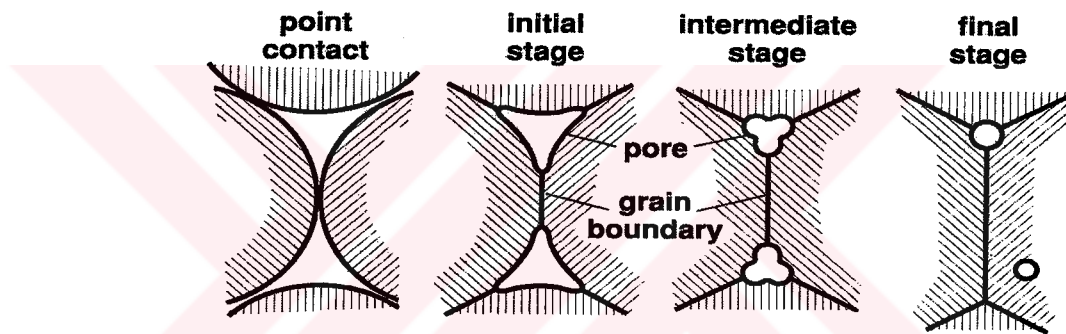


Figure 2.7 The development of the interparticle bond during sintering, starting with a point contact. The pore volume shrinks and the pores become smoother. As pore spheroidization occurs, the pores are replaced by grain boundaries [25]

2.4.6. Liquid Phase Sintering

In the majority of cases the use of liquid phase sintering is related to the desire to produce a very high-density sintered material with little residual porosity. That is, substantial densification is usually associated with liquid phase sintering. In many cases it also yields a very desirable metallurgical structure that favors excellent mechanical properties.

A number of characteristics of typical liquid phase sintering systems are;

- (a) the composition of the alloy is such that according to the appropriate phase diagram there is a solid and a liquid phase present for a significant time at the sintering temperature,
- (b) the solid phase should have a limited solubility in the liquid phase,
- (c) the amount of liquid phase should be small enough so that the shape of the green compact is retained during sintering but large enough so that appreciable densification takes place,
- (d) the particle size of the powder component that is the solid phase during sintering should normally be relatively fine to facilitate rapid densification,
- (e) densification is achieved by sintering and, hence, the compaction pressure may be quite low and relatively unimportant
- (f) in most cases the treatment should yield a sintered compact in which the particles that were solid during sintering are completely surrounded by the phase that was liquid [26].

In liquid phase sintering, densification occurs in stages as sketched in Figure 2.8. Initially, the mixed powders are heated to a temperature where liquid forms. During heating there is solid-state sintering, in part driven by the chemical concentration gradient in the microstructure. Three stages of densification are encountered after the liquid forms: rearrangement, solution-reprecipitation, and final-stage sintering. On liquid formation there is a burst of rearrangement densification, followed by solution-reprecipitation with concomitant grain growth and grain shape accommodation. If there is a high liquid level, full density can be achieved via rearrangement upon liquid formation. On the other hand, at low liquid contents the solid skeleton inhibits densification, requiring the participation of solution-reprecipitation events, where mass transport through the liquid controls densification. Residual final porosity is eliminated by solid-state sintering of the rigid solid skeleton.

With liquid formation there is a densification burst due to the capillary force exerted by the liquid on the solid particles. These grains shrink as solid dissolves into the liquid. Rapidly, the solid grains pack to a higher density, releasing liquid to fill pores between grains. For wetting liquids, the solid-liquid surface energy is lower than the solid-vapor surface energy, resulting in reduced system energy. During rearrangement the compact exhibits viscous response to the capillary action. Full density is possible by rearrangement if enough liquid is formed [32].

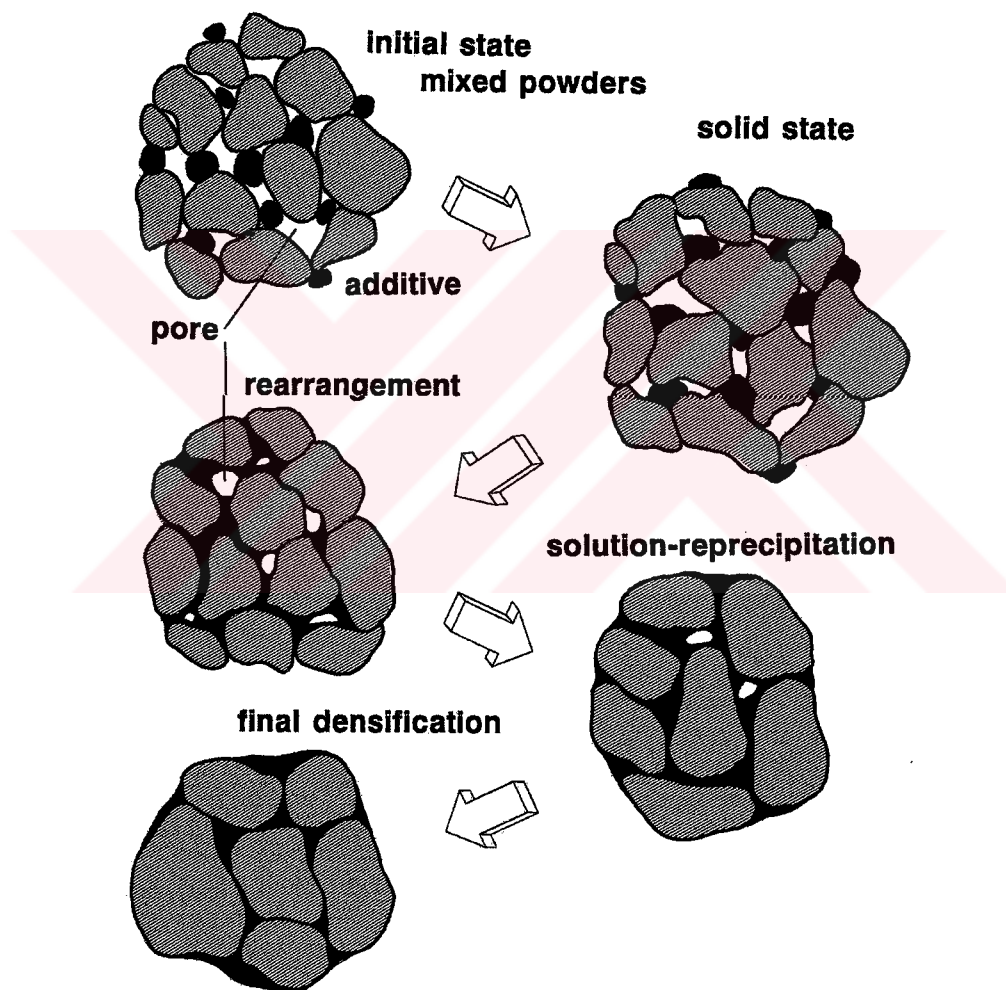


Figure 2.8 Schematic diagram of the classical liquid-phase sintering stages involving mixed powders which form a nonreactive liquid on heating, allowing subsequent particle rearrangement and densification by solution-reprecipitation and solid skeleton sintering [31].

As densification by rearrangement slows, solubility and diffusivity effects dominate. This second stage is called solution-reprecipitation. The solubility of a grain in its surrounding liquid varies inversely with the grain size; small grains have a higher energy and solubility than large ones. The difference in solubilities establishes a concentration gradient in the liquid. Material is transported from the small grains to the large grains by diffusion through the liquid. This process is termed Ostwald ripening. The net result is progressive growth of the larger grains at the expense of the smaller grains giving fewer grains with a larger average size. Solution-reprecipitation not only contributes to grain coarsening but also to densification via grain shape accommodation, allowing a customized fitting together of the growing grains to better fill space.

The final stage of liquid-phase sintering is controlled by densification of the solid structure. Densification is slow because of the rigid skeleton of contacting solid grains. Process dominant in the final stage are also active earlier; however, because it is slow, it is not significant until late in the cycle. Microstructural coarsening continues and the residual pores enlarge if they contain trapped gas, giving compact swelling. In general, prolonged final-stage sintering degrades properties of most liquid-phase sintered materials. Hence, short sintering times are preferred in practice [31].

2.4.6.1. Transient Liquid Phase Sintering

When elemental powder mixtures are sintered at temperatures above the melting point of one of the components, liquid will be present during heating and sometimes at the beginning of the isothermal sintering, but it will disappear eventually if the total composition is such that the equilibrium phase is a solid. Such transient liquid phase sintering is usually a complex process, because liquids may disappear and reappear during heating, and intermetallic phases may be produced intermittently. The alloy systems exhibiting such behavior are, for example, Cu-Sn, Fe-Al, and Cu-Al [33]. Since the wrought aluminum bronze

containing about 10%Al and some Fe or Ni has a high strength and good corrosion resistance, several studies on the liquid phase sintering of Cu-Al compacts have been made which showed an expansion above the eutectic point temperature of 548°C, and various mechanisms have been suggested [34-36].

The requirements for transient liquid phase sintering include solubility between the components, with the final composition existing within a single-phase region at the peak sintering temperature. Generally, the sequence of steps is as follows:

(1) swelling by interdiffusion prior to melt formation (Kirkendall porosity), (2) melt formation, (3) spreading of the melt and generation of pores at prior additive particle sites, (4) melt penetration along solid-solid contacts, (5) rearrangement of the solid grains, (6) solution-precipitation induced densification, (7) diffusional homogenization, (8) loss of melt, (9) formation of a rigid solid structure, and (10) densification by solid state sintering. The actual steps depend on several process variables including particle sizes, amount of additive and hence the liquid, heating rate and maximum temperature [31].

Two phase diagrams of systems, which could be processed by transient liquid phase sintering, are shown in Figure 2.9. In Figure 2.9-a, a low melting temperature additive, A, is used to generate the liquid, yet the overall composition is in the single-phase solid region. The sintering temperature is between the melting temperatures of the two components. Alternatively, in Figure 2.9-b, a eutectic reaction provides the liquid from interdiffusion of the components during sintering. The sintering temperature is greater than the eutectic temperature and the final composition is in the single-phase field. For both cases, the liquid has a high solubility in the solid and disappears with sintering time. This characteristic may induce swelling during heating to the sintering temperature. The densification associated with transient liquid phase sintering depends on the amount of liquid formed and the time the liquid exists.

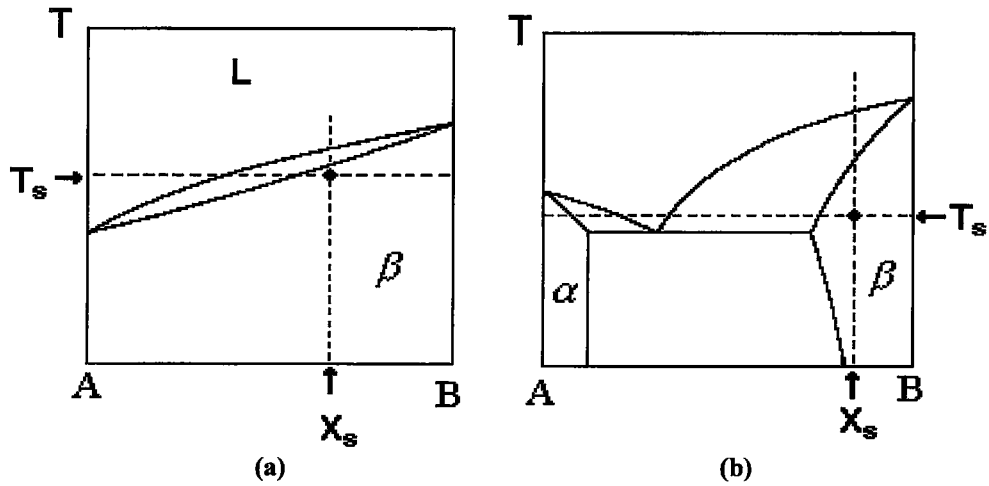


Figure 2.9. Phase diagrams of two systems, which could be processed by transient liquid phase sintering [31]

Problems can arise in transient liquid phase sintering if an intermediate compound forms between the additive and base. A system with an intermediate compound would be expected to give swelling. A high melting temperature compound will inhibit interdiffusion and the formation of the eutectic melt between the compound and the base. Consequently, use of pure A as the additive is counterproductive in this case. Better transient liquid phase sintering occurs from the use of the intermediate compound as the starting additive component [37].

2.4.6.2. Pore Formation and Swelling During Liquid Phase Sintering

As chemical driving forces (free energy of alloy formation) are some orders of magnitude larger than physical ones (reduction of internal surface), it is thermodynamically possible that during alloy formation the porosity of the compact is not lowered but in fact increased.

Of course, the pore formation mechanisms known from steady state liquid phase sintering also occur in transient liquid phase sintering, especially 'pore rearrangement', i.e. liquid phase flow from its original site into the small

capillaries between the solid matrix particles is found in both cases and is described frequently in the literature [38-44], the driving force being the difference in capillary force between the pores containing the binder particles (radius R_1) and the matrix porosity (average radius R_2), if $R_2 < R_1$. The resulting microstructure then consists of a matrix of relatively high density containing pores comparable in size to the original particles of the lower melting component.

This process has been found to occur with steady state as well as with transient liquid phase sintering. In case, however, liquid phase is present during the entire sintering process, or if large amounts of liquid phase are present in the initial stage of sintering, the pores thus generated can be closed. This can occur by particle rearrangement, especially if the particle surfaces are smooth, or by extraction of liquid phase from surrounding areas-melt being available through particle shape accommodation and by growth of the solid particles and resulting in a reduction of retaining capillary forces. In case of transient liquid phase (especially if only low amounts of melt are available), particle rearrangement is not so easy, in part owing to solid particle interlocking. Liquid phase extraction would be contrary to alloy formation and thus is energetically unfavorable. Thus, formation of pores may occur both during sintering with steady state and transient liquid phase, but in the latter case the pores are much more likely to be found also in the sintered product [45].

Since the pores form due to spreading and penetration of the melt away from the additive particle sites, if the initial density is high, liquid flow is inhibited. The greater the initial inhomogeneity in the powder structure, the more swelling occurs, but in turn the peak liquid content is larger and lasts longer, to give more subsequent densification. Pore refilling often does not occur because of as short liquid duration, resulting in large pores in the final microstructure.

There is an effect of heating rate on densification during transient liquid phase sintering. More swelling occurs at slower heating rates due to diffusional

homogenization, which reduces the peak quantity of liquid. The liquid quantity and its duration determine the net shrinkage.

Additionally, during transient liquid phase sintering, solid-state interdiffusion can form an intermediate compound around the additive particles depending on the phase diagram. The intermetallic envelopes inhibit subsequent interdiffusion. The thickness of the intermediate compound initially increases with the square root of time, giving progressive swelling, and may even result in an exothermic reaction which heats the compact. The swelling reaction is most intense just prior to liquid formation. Generally, faster heating rates, smaller particle sizes and lower additive contents give superior sintered properties for transient liquid phase sintering [31].

2.5. POWDER METALLURGY OF Cu-BASED ALLOYS

The use of copper in the powder metallurgy industry dates back to the 1020's, when the porous bronze bearings became commercialized. These self-lubricating bearings, which are the oldest application of porous P/M parts, were developed independently in the research laboratories of General Motors Corp. and Bound-Brook Oilless Bearing Co. Currently, these bearings account for the major portion of P/M copper and copper alloy applications. Other important applications for copper and copper-based P/M materials include friction materials, brush, filters, structural parts, electrical parts, additives to iron powders, paints, and pigments.

Physical and mechanical properties of copper and copper alloy P/M parts are comparable with cast and wrought copper-based materials of similar composition on a density-related basis. Additionally, P/M processing permits flexibility in part design. For example, P/M copper parts may vary in density from the low density typical of self-lubricating bearings or filters to the near-theoretical density of wrought parts.

Copper powder containing more than 99% Cu is available commercially. Powder metallurgy parts produced from these powders have electrical conductivities of 80 to 95% IACS in the as-pressed and sintered condition. Further densification provides higher conductivities, approaching 100% IACS. Copper P/M parts provide an added benefit in the production of electronic and electrical components that require superior electrical or thermal conductivity.

Copper and copper alloy powders, which exhibit excellent ductility representative of wrought copper grades, enjoy wide usage in industrial applications. Their primary application is in the production of self-lubricating bearings. This example illustrates the advantage of producing a part with controlled interconnected and surface-connected porosity through P/M techniques. A similar production method is used in the manufacture of metallic bronze filters.

Alloyed with tin, zinc, nickel, and/or other elements, copper powder is used for many structural parts and friction materials. Brasses, bronzes and other copper alloys produced by P/M methods exhibit physical and mechanical properties comparable to their cast and wrought counterparts. Copper also is used as an alloying element in iron powder components to enhance mechanical properties and control dimensional changes during sintering.

The four methods for producing unalloyed copper powders are atomization, electrolysis, hydrometallurgy, and oxide reduction.

Atomized particles may be annealed in a reducing atmosphere to minimize surface oxide formed during atomization. Copper powder can be produced as either spherical or irregular in shape. Purity, depending on processing technique, exceeds 99%. Electrolytic copper powder is produced by electrodeposition of copper to obtain a non-adherent powder deposit, rather than a smooth, continuous adherent layer. Hydrometallurgy is used to produce copper powder from copper cement, concentrates, or scrap copper. Copper is leached from these materials with sulfuric

acid or ammoniacal solutions, and the resulting solution is separated from the residue by filtration. Copper is precipitated as powder. With oxide reduction method, oxides are ground to controlled particle sizes and then reduced in gas atmospheres containing carbon monoxide, hydrogen, and cracked natural gas at temperatures below the melting point of copper.

Cu-base alloys are produced either from elemental powders or from prealloyed powders. Preblended powders are mixtures of selected compositions, with or without lubricant, that form the desired alloy during sintering. Cu-based prealloyed powders are also produced by the atomization of the alloy material. In addition to that, prealloyed powders are produced by sintering a preblend, which is followed by a grinding operation to produce the desired powder characteristics.

Alloy powders are available in various compositions, including brasses ranging from 95Cu-5Zn to 60Cu-40Zn and nickel silvers, tin bronzes, aluminum bronzes, and beryllium bronzes.

Although, in the consolidation of copper and copper based alloy powders, usually, a closed die is used other methods such as hot pressing roll compaction, isostatic pressing, extrusion and forging may also be applied. As it was described earlier, by the application of the pressure firstly, particles rearrange with minimal deformation. Next, contacts between particles undergo an elastic compression, which is followed by the plastic deformation at the contacts to form increasingly larger areas and finally massive deformation of total powder mass occurs. For successful compaction of pure copper powders to form P/M parts, the applied pressures should be relatively low. This is important in order to permit the escape of gases and water vapor formed by internal reduction of copper oxides on sintering in a reducing atmosphere. If the initial compacting pressure is too high, the center of the compact will not sinter. For this reason, in the compaction of pure copper powders, pressures in the range of 205 to 250 MPa should be used. However, the compacting pressures of prealloyed Cu-based powders are higher

due to their higher yield strengths and work hardening rates compared to pure copper powder or premixed powders.

The compacted copper and copper alloy powders should be sintered to obtain bonding between particles and hence higher densities and strengths as it was discussed in the previous section. The mechanisms of densification during sintering are viscous flow, volume diffusion, plastic flow, evaporation-condensation and surface diffusion. Only the first three mechanisms are capable of producing shrinkage, while all of these mechanisms may produce bonding. However, in the case of a metal such as copper it seems that viscous flow may exhibit quasi-viscous behavior, if stress motivated volume diffusion currents occur between suitable sources and sinks [46]. The effective sintering range of copper or Cu-based powder is 750 to 1000°C.

If alloys are desired to be produced from elemental copper powders by adding constituents like Al, Zn or Sn into the copper powder, at the effective temperature of sintering, liquid formation of the low melting constituent occurs. As a result of this, the process termed as liquid phase sintering is encountered causing the growth and shrinkage of the compacts. However, in such systems in which copper is the main constituent or the additive element, some additives like carbon in the form of graphite can control the dimensional changes. For example, in the iron-copper system, such an addition increases the proportion of the liquid phase by promoting the formation of a ternary eutectic which results in less net expansion. However, in the copper-tin system, the graphite inhibits sintering by mechanical separating the components of the compact, which results in more net expansion.

2.6. POWDER METALLURGY OF Cu-BASED SMA

Shape memory alloys are conventionally produced by melting and casting methods as previously mentioned. However, powder metallurgy is extensively being used as an alternative production method with the main purposes of controlling the alloy composition and preventing grain growth.

In general, a minor variation in chemical composition will cause an unexpectedly large shift in the transformation temperatures of the shape memory alloys. The conventional way of preparing shape memory alloys from constituent elements by melting and casting simply cannot control the alloy composition with enough accuracy to hold the transformation temperature within the desired range. However, in the study of Jean et al, it was found that P/M could be a promising method to produce shape memory alloys with predictable transformation temperatures by obtaining a strict control on the chemical composition [47].

For the preparation of shape memory alloys the conventional casting method has difficulties in controlling the grain size. Coarse grains will weaken the mechanical properties of alloys. It has been reported that mechanical alloying and powder metallurgy with hot isostatic press can be used to fabricate Cu-based shape memory alloys. Powder metallurgy can reduce the hot working process in fabricating the near-net shape products and usually give better control of grain size [7].

Production of TiNi shape memory alloys by powder metallurgy has been widely investigated. However, in recent years, Cu-based shape memory alloys have been extensively developed because of their more competitive cost and easier fabrication processes.

The main problems in the actual utilization of Cu-based shape memory alloys are mainly due to their low thermal stability and unsatisfactory mechanical strength.

They often suffer from martensite stabilization and finally lose the thermoelastic properties. Moreover, intergranular cracking usually occurs in Cu-based shape memory alloys during the manufacturing process and in service. Hence, improving the thermal stability and mechanical properties are important issues for the prospect of Cu-based shape memory alloys [48].

Lu et al. [5] investigated the production of Cu-Zn-Al shape memory alloys by powder metallurgical methods. The prealloyed powders with compositions Cu₇-Zn₃₀, Cu₈₆Zn₁₄ and elemental Al powders were used directly to produce shape memory alloy powder with the required composition. The powders were mechanically alloyed under Argon atmosphere to reduce oxidation. As a result of this work, it was concluded that, shape memory powders for the production of shape memory alloys could be prepared using the mechanical alloying method.

Jean et al. [6], Tang et al. [7] and Duerig et al. [8] have studied on the production of Cu-Al-Ni shape memory alloys starting from pre-alloyed powders. The main aim was to reduce the grain size of the alloys in order to increase the mechanical properties. In the study of Jean et al., the prealloyed powders were hot pressed and sintered in a vacuum of 10⁻² Pa at 900°C. However, Tang et al. and Duerig et al. applied cold compaction to consolidate the prealloyed powders. Tang et al. applied a pressure of 900MPa to obtain disc-shaped green compacts and these compacts were sintered at 950°C for 20 hrs under Argon gas atmosphere followed by furnace cooling. Duerig et al. applied hot swaging to the cold compacted and sintered compacts. As a result of these studies, the grain size of the alloys was reduced to a value well below 2µm, which is the average value obtained by conventional casting. Additionally, the shape memory alloys produced by the powder metallurgical methods described above revealed the same shape memory properties with the specimens that are produced by casting method.

CHAPTER 3

EXPERIMENTAL PROCEDURE

3.1. MATERIAL USED

For the preparation of all the specimens, pure elemental powders of Cu, Al, and Ni were used. The copper powder, which has an average particle size of 50 μm , was supplied from Merck (art-2715). Ni powder with two different powder sizes (5 μm and 46 μm) was supplied from Strem Chemicals. A commercial Al powder was used which has an average particle size of 26.2 μm . The effect of particle size differences of the constituents was out of concern of this study.

3.2. EXPERIMENTAL SET-UP AND TECHNIQUE

3.2.1. Mixing

For all specimens prepared throughout this study, elemental powders were hand mixed in alcohol to obtain a uniform powder distribution. The mixed powders were consolidated by cold compaction in a semi-wet condition to prevent powder settling, which tends to occur due to particle size differences.

3.2.2. Cold Compaction

Consolidation of metal powders was carried out in cylindrical, single-end die, using a manual hydraulic press. The steel die had a diameter of 15.2 mm and the compacted specimens had a thickness of 3 to 4 mm. The pressure was in the range 300-700 MPa.

3.2.3. Sintering

The green compacts of all Cu, Al and Ni powder mixtures were sintered in a horizontal tube furnaces. The hot zone of the furnace was determined and the specimens were placed at the center of the hot zone. Strict temperature control was obtained during sintering operations, by using a second thermocouple other than the thermocouple of the tube furnace. This second thermocouple was placed into the ceramic tube just above the specimen.

Sintering was carried out under hydrogen atmosphere, which is a reducing atmosphere for the main constituents copper and nickel. The possible moisture of the hydrogen gas was removed by flowing the gas through a silica gel, before being introduced into the furnace.

3.2.4. Hot Rolling

Hot rolling equipment consists of a plate-thread rolling mill coupled with a horizontal tube furnace. The rolling mill was supplied from Cavallin SRL with a catalogue number of M2200. The rolling mill has a 1.5 HP motor leading to a production rate of 3.6 to 6.9 m/min. the rolls of the machine have a diameter of 65 mm and a width of 120 mm. Maximum thickness which can be rolled is 16 mm and the opening of the rolls can be adjusted with a sensitivity of 1/20th of a millimeter. The furnace that permits a hot rolling operation was specially designed and constructed in the Department, so that the specimens could be fed in to the

rolling mill without much heat loss. The furnace is a horizontal type steel tube furnace. The operation temperature is controlled with a K-type thermocouple, which is placed under the insulating material just above the hot zone of the furnace.

The specimens were hot rolled at 900°C by giving approximately 15% reduction in thickness at each step, and were examined metallographically both before and after hot rolling.

3.3. INVESTIGATED SYSTEMS

The Cu-Al specimens were prepared at three different compositions, namely Cu-6^w/₀ Al, Cu-10^w/₀ Al, and Cu-14^w/₀ Al from elemental powders of Al and Cu. All the specimens were sintered under H₂ atmosphere for 1 hour, at three different temperatures (Table 3.1).

Table 3.1. Investigated Cu-Al systems and sintering temperatures

	Composition	Sintering Temperatures (°C)		
		850	900	950
S1-1	Cu-6 ^w / ₀ Al	✓	✓	✓
S1-2	Cu-10 ^w / ₀ Al	✓	✓	✓
S1-3	Cu-14 ^w / ₀ Al	✓	✓	✓

Stepwise sintering was also carried out to minimize pore formation in Cu-12^w/₀ Al specimens. In this type of sintering, furnace is heated to the first sintering temperature, T_1 , at a rate of 15 °C/min. When the sintering at T_1 is completed, the furnace is heated to the second sintering temperature (T_2), and kept at that temperature for a definite time (Figure 3.1). The temperatures T_1 and T_2 were different for various stepwise sintering routes.

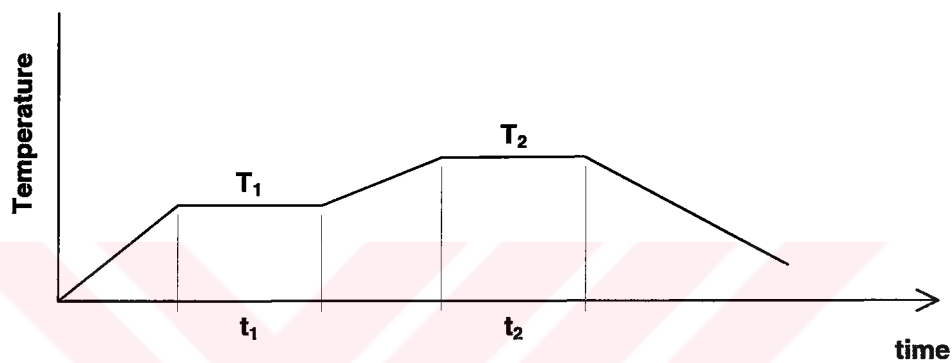


Figure 3.1. Schematic representation of the stepwise sintering

Although soaking the specimen at T_1 is named as sintering, the main purpose in this first step was different. Rather than sintering, it was aimed to give enough time for mutual diffusion of Cu and Al powders.

All the specimens of the sintering studies were examined metallographically, and their densities were measured before and after sintering.

The second binary system, Cu-Ni, was also investigated to observe the densification behavior and microstructure change upon sintering at different temperatures.

Ni powder with two different sizes was used i.e., fine Ni powder (5 μm) & coarse Ni (46 μm). The cold compacts were sintered at three different temperatures, which are below the solidus temperature of the corresponding composition. The sintering parameters investigated in Cu-Ni system is tabulated in Table 3.2.

Table 3.2. The investigated Cu-Ni systems and their sintering temperatures

Composition	Ni Size (μm)	Sintering Temperatures ($^{\circ}\text{C}$)					
		850	900	950	1000	1050	1100
Cu-4 ^w / ₀ Ni	5	✓		✓		✓	
	46	✓		✓		✓	
Cu-8 ^w / ₀ Ni	5		✓		✓		✓
	46		✓		✓		✓

Densities of the specimens were measured before and after sintering. They were examined metallographically after sintering.

The last sintering attempt was on Cu-Al-Ni ternary system. The specimens were prepared at a composition of Cu-12^w/₀Al-4^w/₀Ni and they were compacted at 700 MPa. The sintering routes of the investigated systems are given in Table 3.3.

Table 3.3. Sintering routes of the hot rolled Cu-Al-Ni system

Sintering Routes	500 °C (2 hrs)	500 °C (2 hrs) + 1000 °C (1 hr)	1000 °C (1 hr)
Cu-12^w/₀Al-4^w/₀Ni	✓	✓	✓

Hot rolling studies were carried out on Cu-12^w/₀Al, Cu-4^w/₀Ni and Cu-12^w/₀Al-4^w/₀Ni specimens.

Cu-12^w/₀Al specimens were compacted at different pressures in a range of 300-500 MPa, and were sintered by following different routes before hot rolling.

The hot rolled Cu-Ni specimens were prepared at a composition of Cu-4^w/₀Ni. They were prepared with two different Ni powder size and were compacted at 700 MPa. They were hot rolled after sintering at various temperatures.

Cu-Al-Ni system was also hot rolled after sintering. The specimens were prepared at a composition of Cu-12^w/₀Al - 4^w/₀Ni and were compacted at 700 MPa.

Finally, γ -Al₂O₃ is added as a grain refining element in small amount (0.3^w/₀) and its effect is observed on both the Cu-Al binary, and the Cu-Al-Ni ternary systems. The γ -Al₂O₃ powder had 0.05 μ m size and it was mixed with the other constituents in alcohol and the mixture was cold pressed at 300 MPa in a semi-wet condition. The investigated systems are listed in Table 3.4.

Table 3.4. Sintering temperatures and compositions of the investigated systems for grain refining studies

Code	Composition (w/o)				Sintering Temperatures (°C)			
	Cu	Al	Ni	γ -Al ₂ O ₃	850	900	950	1000
12Al	88	12	-	-	✓	✓	✓	✓
12Al-0.3G	87.7	12	-	0.3	✓	✓	✓	✓
12Al-4Ni	84	12	4	-	✓	✓	✓	✓
12Al-4Ni-0.3G	83.7	12	4	0.3	✓	✓	✓	✓

Densities of the specimens were measured both before and after sintering, by Archimedes' principle. All the specimens were examined metallographically.

3.4. DENSITY MEASUREMENT

The density measurements of the samples were based on Archimedes' principle, since the specimens showed swelling and the sintered dimensions of the compacts were non-uniform. The Archimedes' Principle states, "Any body completely or partially submerged in a fluid is buoyed up by a force equal to the weight of the fluid displaced by the body".

The weight of a body, W , can be given as;

$$W = m \times g \quad (3.1)$$

Where m is the mass of the body and g is the gravitational acceleration. The small buoyant force of air is neglected.

When the specimen is immersed in water, it experiences an upward buoyant force, F , equal to the weight of water displaced. This force is,

$$F = W = m_w \times g = V \times \rho_w \times g \quad (3.2)$$

Where m_w is the mass of water displaced, V is the volume of the specimen and ρ_w is the density of water, which is 1 gr/cm^3

The actual weight of the specimen decreases by an amount when it is immersed in water, since it causes overflow of water. The upward buoyant force acting on the specimen is the difference between the actual weight of the specimen and the weight of specimen when immersed in water.

$$F = W_{\text{actual}} - W^* = (m \times g) - (m^* \times g) \quad (3.3)$$

Where W^* is the weight of the specimen in water, and m^* is the mass of the specimen in water.

Since the buoyant force is also equal to the weight of the water that is displaced, the equations 3.2 and 3.3 are equal;

$$V \times \rho_w \times g = (m \times g) - (m^* \times g);$$

$$V \times \rho_w \times g = (m - m^*) \times g$$

$$V = (m - m^*) / \rho_w$$

$$\text{Since } \rho_w = 1 \text{ gr/cm}^3;$$

$$V = (m - m^*) \quad (3.4)$$

In our case, since the sintered specimens contained pores- that will be mentioned in detail in the following sections- they were coated with a polymeric fluid, to

prevent the water to fill the pores. When the Archimedes' principle is applied to those specimens, some details should be taken into account.

V, which is calculated from the equation 3.4, is the volume of the body immersed into water. But this body includes the volume of the specimen and the volume of the polymeric fluid. To find the volume of the specimen, we should find the volume of the polymeric fluid, and then subtract it from the total volume obtained from equation 3.4.

$$V_{\text{fluid}} = m_{\text{fluid}} / \rho_{\text{fluid}} \quad (3.5)$$

The actual mass of the specimen is measured both before coating and after coating with the polymeric fluid. So by finding the difference between these two values, we can find the mass of the polymeric fluid. We take density of fluid approximately, 1 gr/cm³ since it is a polymer.

$$V_{\text{specimen}} = V - V_{\text{fluid}} \quad (3.6)$$

Once the volume of the specimen is calculated, the density can also be calculated with the equation;

$$\rho_{\text{specimen}} = m_{\text{specimen}} / V_{\text{specimen}} \quad (3.7)$$

The error limit of the density measurements were analyzed and determined as 2%.

3.5. METALLOGRAPHIC EXAMINATION

The microstructural characterizations of the specimens were done by using Olympus MG optical microscopes. Colored and black-white micrographs were taken by using Nikon FDX-35 camera that is connected to Nikon Optiphot-100 type microscope. The specimens were examined both in as-polished and etched conditions. 5% $[\text{NH}_4]_2\text{S}_2\text{O}_8$ (ammonium oxide persulfate) solution was used as the etching agent during the examinations.

Scanning electron microscope studies were carried out using a Jeol 6400 Scanning Electron Microscope. The spot analyses were performed using the 'Northern Tracor' EDS analysis system, which was attached to the scanning electron microscope.



CHAPTER 4

EXPERIMENTAL RESULTS

The initial attempt was to investigate the sintering behavior of Cu-Al, Cu-Ni and Cu-Al-Ni powder mixtures. All the mixtures were prepared from elemental powders.

4.1. SINTERING STUDIES ON Cu-Al SYSTEM

Cu-Al powder mixture forms the basis of both Cu-Al-Ni (Cu-12^{w/o} Al-4^{w/o} Ni) and Cu-Zn-Al (Cu-7^{w/o} Al-19.5^{w/o} Zn) shape memory alloys. For this reason, in the first part of the study, sinterability of Cu-Al system was investigated.

As it is already mentioned in the previous chapter, Cu-Al binary alloys have been prepared by hand mixing elemental powders of Cu and Al in alcohol. Then the mixture was cold compacted at 300 MPa. In the first part of this study, Cu-Al compacts of three different compositions in the range of 6-14^{w/o}Al were prepared. All the specimens were sintered in a temperature range of 850-950°C, under H₂ atmosphere. Sintering time was kept constant at 1 hour. Table 4.1 gives the details of the investigated Cu-Al powder compositions and their sintering temperatures.

Table 4.1 The compositions and sintering temperatures of Cu-Al system

	Composition	Sintering Temperatures (°C)		
		850	900	950
S1-1	Cu-6 ^w / ₀ Al	✓	✓	✓
S1-2	Cu-10 ^w / ₀ Al	✓	✓	✓
S1-3	Cu-14 ^w / ₀ Al	✓	✓	✓

Table 4.2 and Figure 4.1 shows the densities of Cu-Al compacts after sintering at various temperatures. As can be seen from Figure 4.1, with an increase in sintering temperature, there is no significant change in densification. The % theoretical densities (%T.D.) of green compacts are in the range 70-75 %T.D. The sintered densities show practically no change with an increase in sintering temperature.

Table 4.2. The densities of the Cu-Al specimens before and after sintering

Investigated systems	Density before sintering (%T.D.)	Density after sintering at; (%T.D.)		
		850°C	900°C	950°C
Cu-6^w/₀Al	74	77	74	75
Cu-10^w/₀Al	71	71	72	71
Cu-14^w/₀Al	70	70	68	70

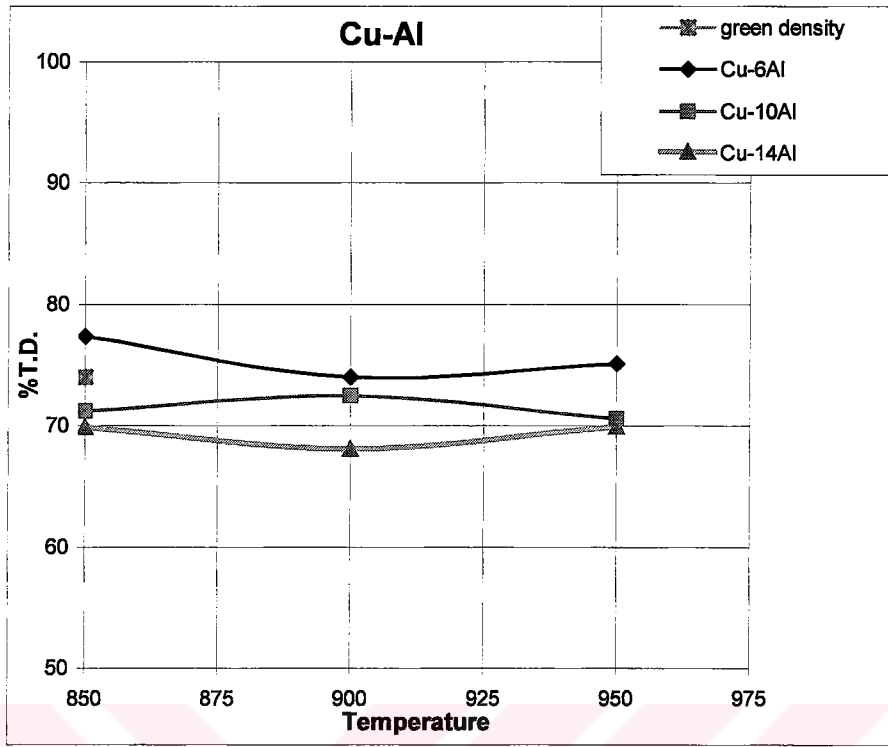


Figure 4.1. The change in density of cold compacted and sintered Cu-Al specimens as a function of sintering temperature

After the sintering processes, all the specimens were prepared for metallographic examination and examined with optical and scanning electron microscopes in either as-polished, or polished and etched condition. As a result of these metallographic examinations, pores were observed in all of the specimens. For example, Figure 4.2 belongs to Cu-6^w/₀Al specimen, compacted at 300 MPa and sintered at 850°C for 1 hour. The black spot is the pore present at the original sites of Al powder.

On the other hand, the microstructure of Cu-14^w/₀Al specimen is shown in Figure 4.3. A comparison of Figure 4.2 and 4.3 shows that the amount of pores increase with an increase in ^w/₀Al.

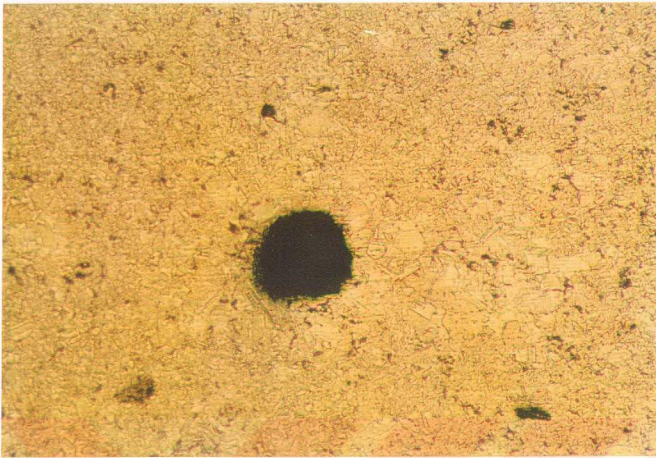


Figure 4.2. The optical micrograph of Cu-6^w/₀Al specimen sintered at 850°C

X150

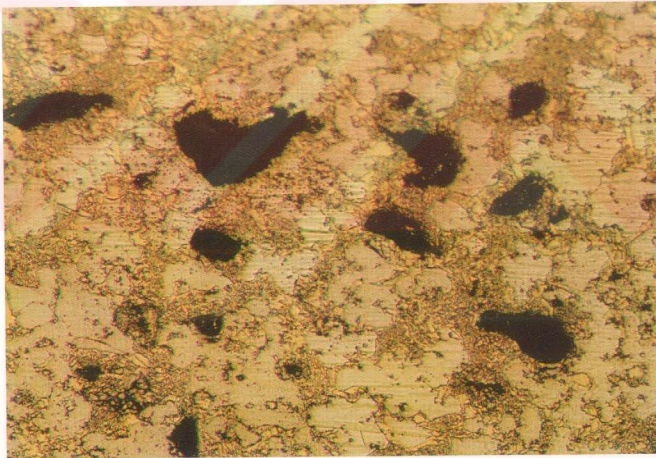


Figure 4.3. The optical micrograph of Cu-14^w/₀Al specimen sintered at 850°C

X150

As shown by microstructural observations, pore formation, observed in the previous experiments, is still a big problem in Cu-Al specimens. The reason for pore formation is predicted to be the compositional solidification of liquid Al, which forms during sintering [48,49]. The major factor contributing to the pore formation is the difference in the densities of the liquid and the solid formed in place of it during solidification. The solidification in Cu-Al system occurs by an isothermal composition shift during sintering. Pure aluminum regions transform into liquid at the initial stages of sintering, and this liquid solidifies by the rapid diffusion of copper atoms into it during later stages. As it is well known fact that solids are denser than liquids, with a few exceptions, the solidified regions occupy less volume than the liquid does and so pore formation takes place in these regions [48].

Depending on previous investigations, it can be stated that formation of a liquid phase in Cu-Al system initiates pore formation. So, in order to prevent pore formation, we should prevent the formation of liquid Al as well. For this purpose, solid-state sintering studies were carried out on Cu-Al system. Specimens with a composition of Cu-12^w/₀ Al were prepared for this purpose. This Al concentration corresponds to the same concentration in the ternary system i.e. Cu-12^w/₀ Al- 4^w/₀ Ni, which reveals shape memory behavior. Several specimens were sintered below the eutectic temperature of 548^oC. This temperature corresponds to the level at which first liquid appears throughout the Cu-Al phase diagram (Figure 4.4).

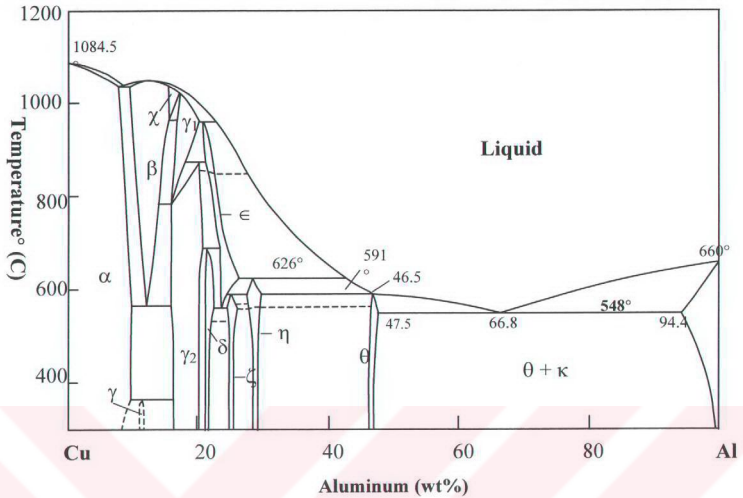


Figure 4.4. Cu-Al Binary Phase Diagram

Although the specimen composition, which is Cu-12 wt% Al, corresponds to the β phase region of the phase diagram and the first liquid should appear at a temperature around 1050°C, in our study the mechanism is somewhat different. The specimens produced in this study are composed of pure powders of Cu and Al. During sintering, Cu atoms diffuse into Al. New phases start to form by diffusion, around the Al powder. When we look at the Al rich side of the Cu-Al phase diagram, as the Cu diffuses into Al, θ phase should form first. At this region, the first liquid forms at 548°C, which is the eutectic temperature. So, any specimen exposed to a temperature higher than 548°C will enhance liquid phase formation. In order to prevent the formation of liquid Al, sintering should be carried at a temperature below 548°C.

As we already mentioned above, with the diffusion of Cu atoms into Al powder, the Cu concentration in Al powder increases. This would mean that Al powder is not pure any more, but its composition is shifted to Cu rich part of the Cu-Al phase diagram. As a result, the liquidus temperature will increase and formation of a liquid phase within the Al powder will become more difficult. Consequently, the structure can be sintered at higher temperatures without liquid formation, if the sintering is carried out stepwise and the temperature is always kept below liquidus line.

For this purpose, firstly Cu-12 ^w/₀ Al specimen was sintered at 530°C for 1 hour and then, at 575°C for 1 hour under H₂ atmosphere. However, the pores could not be eliminated and the diffusion was incomplete.

Since the structure was porous, it is concluded that, liquid phase has formed at the second stage of sintering, i.e. at 575 °C. To prevent the formation of liquid Al, the time for solid-state sintering, i.e. sintering at a temperature below eutectic was increased. By increasing the time, it was expected that, the composition of Al powder could be shifted more to the Cu-rich side of the phase diagram. Therefore, formation of a liquid phase would be less probable when sintering temperature is increased. As a result, the structure would be less porous. For this purpose, the Cu-12 ^w/₀ Al specimen was sintered at 500°C for 2 hours and then, at 550°C for 1 hour. As can be seen in Figure 4.5, a stepwise sintering could not eliminate the pores, but the porosity was reduced slightly.

So, new sintering studies were carried out at 500°C, to provide solid state sintering, in order to examine the reason of porosity.

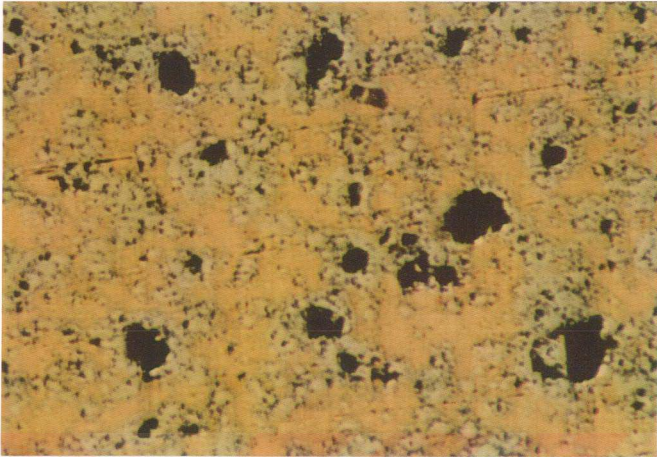


Figure 4.5. The optical micrograph of Cu-12^w/₀Al, 500°C 2 hours + 550°C 1 hour X75

It is a well-known fact that, compaction pressure has significant effects on green and sintered densities of powder metallurgy parts. So, as a second attempt, the compaction pressure was changed during the production of Cu-Al specimens for the solid-state sintering studies. The Cu-12^w/₀ Al specimens were compacted at two different pressures of 300 and 500MPa, and then were sintered at 500°C for 1 hour and 5 hours.

The corresponding sintering times and compaction pressures of the stepwise sintered specimens are given in Table 4.3.

Table 4.3. Sintering routes, compaction pressures and density values of the investigated Cu-12^{wt}%Al specimens

Specimen		S2-1	S2-2	S2-3	S2-4	S2-5	S2-6
Sintering Route	530°C (1 hr) + 575°C (1 hr)	✓					
	500°C (2 hrs) + 575°C (1 hr)		✓				
	500 °C (1 hr)			✓		✓	
	500 °C (5 hrs)				✓		✓
Compaction Pressure	300 MPa	✓	✓	✓	✓		
	500 MPa					✓	✓
Density (%T.D.)	Before sintering	70	70	70	70	75	75
	After Sintering	56	55	59	59	72	72

In Figures 4.6 and 4.7, which belong to Cu-12^{wt}%Al specimens sintered at 500°C, the pores can be clearly seen as black spots. Around the pores, an intermetallic layer (gray), which is most probably CuAl₂, can be seen as well. The specimen compacted at 500 MPa and sintered at 500°C for 5 hours (Figure 4.6), reveals that, larger pores are located at the original Al powder sites.

In Figure 4.7, the microstructure of the specimen compacted at 700 MPa and sintered at 500°C for 1 hour can be seen. This structure also contains pores at the original Al powder sites. But, different from Figure 4.6, pores in this microstructure are smaller in amount and size.

These two microstructures bring the idea of Kirkendall effect, possibly taking part during solid state sintering. First of all, we would not expect to observe pores after solid state sintering (i.e. sintering below the eutectoid temperature), if the pore formation was only due to formation of liquid Al. There can be another mechanism contributing to pore formation, and this mechanism can be based on diffusion, since sintering is carried out in solid state.

Secondly, if Figures 4.6 and 4.7 are compared, it can be seen that, as solid state sintering time is increased, the amount and size of the pores also increase. Since Kirkendall effect is based on diffusion and difference between the mutual diffusivities of the constituents, the increased porosity with increased time can support this idea.

The Cu-12^w/₀Al specimen, compacted at 500MPa and sintered at 500°C for 5 hours, was investigated under scanning electron microscopy as well (Figure 4.8). A pore at the original site of an Al powder can be seen much more easily under S.E.M. (Figure 4.8-a). An irregular region located around the pore can be clearly seen at a higher magnification (Figure 4.8-b). An E.D.S. analysis taken from this region indicated that, these regions have a composition of 76 ^w/₀Cu- 24 ^w/₀Al.

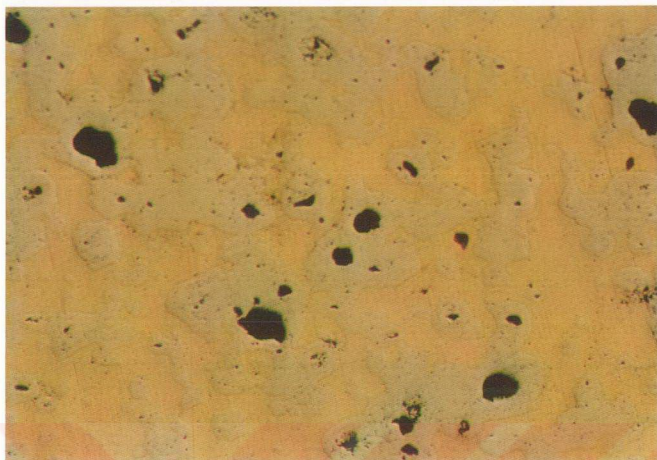


Figure 4.6. The optical micrograph of Cu12^w/₀Al, sintered at 500°C for 5 hours

X75

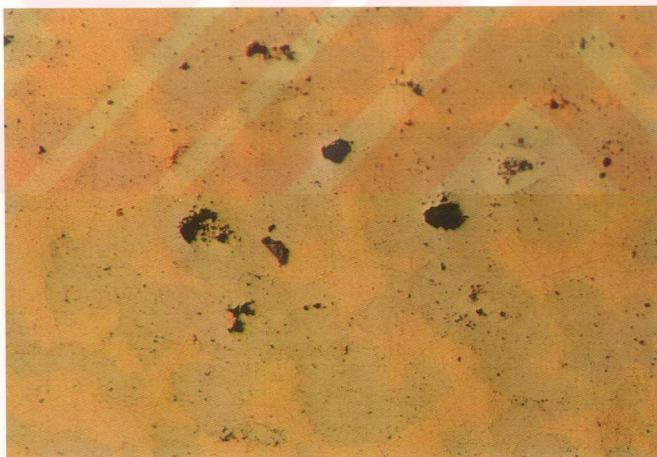
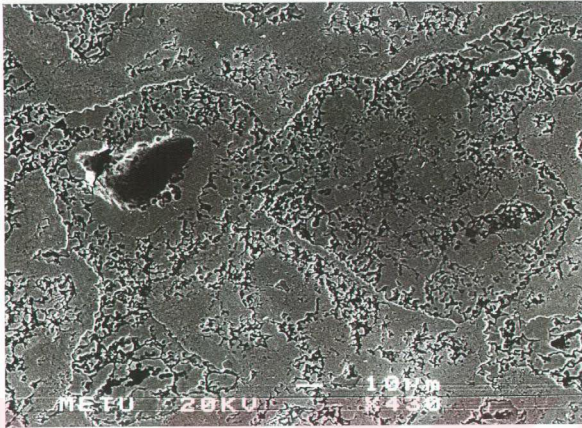
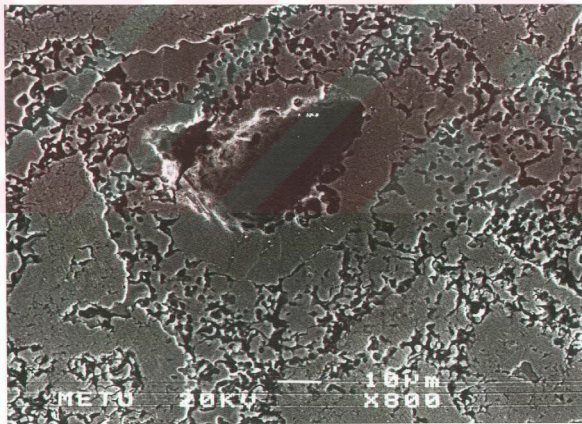


Figure 4.7. The optical micrograph of Cu-12^w/₀Al, sintered at 500 °C for 1 hour

X75



a) x430



b) x800

Figure 4.8. The appearance of a pore under S.E.M. which is taken from Cu-12^{wt}%Al specimen, sintered at 500°C for 5 hours.

The microstructural studies and as-sintered density values obtained after compacting at 300 and 500 MPa pressures has indicated that, compaction pressure has significant effect on porosity of the Cu-Al compacts. So, it is thought that, compacting at much higher pressures and sintering at higher temperatures would further reduce the porosity.

For this purpose, Cu-12 % Al specimens were cold compacted at four different pressures and sintered at two different temperatures for 1 hour. The sintering temperatures, compaction pressures and the density values are given in Table 4.4.

Table 4.4. Sintering temperatures, compaction pressures and density values of the Cu-12 % Al specimens

	Sintering Temperature (°C)		Compaction Pressure (MPa)				Green Density (%T.D.)	Sintered Density (%T.D.)
	950	1000	300	500	600	700		
S3-1	✓		✓				70	71
S3-2	✓			✓			75	74
S3-3	✓				✓		77	76
S3-4	✓					✓	79	78
S3-5		✓	✓				70	76
S3-6		✓		✓			75	77
S3-7		✓			✓		77	78
S3-8		✓				✓	79	79

Density measurements of the specimens were done before and after sintering by Archimedes' principle. The results are as seen in Figure 4.9.

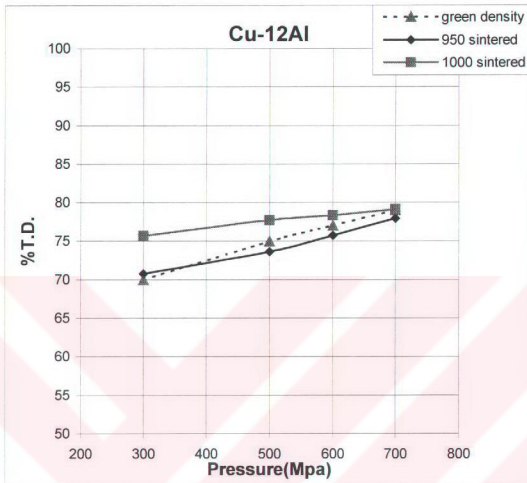


Figure 4.9. Change in density of the cold compacted and sintered Cu-12%Al specimens as a function of temperature.

As seen in Figure 4.9, compaction pressure affects the final densities of the specimens. A higher compaction pressure yields not only higher green densities, but also higher as-sintered densities. The specimens sintered at 1000°C showed an increase in densities upon sintering at every compaction pressure, while the specimens sintered at 900°C showed no significant change in density after sintering.

From the obtained microstructures it was observed that, the specimens compacted at higher pressures yield less amount of porosity and show reduction in pore size. As a result, the optimum compaction pressure was determined as 700 MPa and sintering temperature as 1000 °C, for the production of the Cu-Al binary alloy. The binary system prepared at a composition of Cu-12 % Al were compacted at 700 MPa and were sintered by following different routes. The sintering routes and the specimens are listed in Table 4.5.

Table 4.5. Sintering routes and the densities of the Cu-12 % Al specimens compacted at 700 Mpa

Cu-12 % Al	500 °C (2 hours)	500 °C (2 hours) + 1000 °C (1 hour)	1000 °C (1 hour)
Density before sintering (%T.D.)	78	78	78
Density after sintering (%T.D.)	71	73	79

Either a single-stage sintering below the eutectic temperature, or a stepwise sintering does not contribute much to the final densities. Swelling occurs in Cu-Al specimens. However, no swelling is observed for the specimens sintered at 1000°C.

As a concluding remark, it can be stated that, the pores in Cu-Al mixtures could not be eliminated upon sintering. Either stepwise or single stage sintering does not contribute to the final densities. Especially, powder mixtures heated below eutectic temperature, i.e. 548 °C, has shown swelling.

4.2. SINTERING STUDIES ON Cu-Ni SYSTEM

As mentioned before, the Cu-Ni powder mixtures were prepared at two different compositions from pure powders of Cu and Ni by cold compacting at 300 MPa. Ni powder with two different sizes was used. The cold compacts were sintered at three different temperatures. These sintering temperatures were below the solidus temperature of the corresponding composition as can be seen in the phase diagram (Figure 4.10). It can be stated that sintering was solid state.

Table 4.6 gives the details of composition & Ni powder size of Cu-Ni powder mixtures and their sintering temperatures.

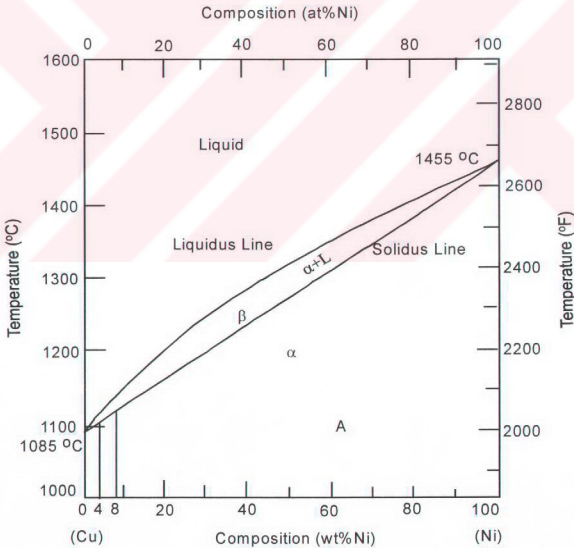


Figure 4.10. Cu-Ni Binary Phase Diagram

Table 4.6. Compositions, powder size, and sintering temperatures of Cu-Ni system.

Comp osition	Ni Size (μm)	Sintering Temperatures ($^{\circ}\text{C}$)					
		850	900	950	1000	1050	1100
Cu-4 ^w / ₀ Ni	5	✓		✓		✓	
	46	✓		✓		✓	
Cu-8 ^w / ₀ Ni	5		✓		✓		✓
	46		✓		✓		✓

As an initial attempt, the Cu-4^w/₀Ni powder mixture was sintered at temperatures 850°C, 950°C, and 1000°C. The change in densities of specimens with respect to sintering temperature is given in Figure 4.11. The densities of green compacts prepared from either fine Ni powder (5 μm) or coarse Ni powder (46 μm), were approximately 77%T.D. The densities of specimens were substantially increased after sintering at 850°C. The attained densities were in the range 86%-92%T.D. (Table 4.7). Sintering at higher temperatures (950°C, 1050°C), did not increase the density significantly.

Table 4.7. The densities of Cu-4^w/₀Ni specimens before and after sintering.

Cu-4 ^w / ₀ Ni	Density before sintering (%T.D.)	%T.D. after sintering at;		
		850°C	950°C	1050°C
Fine Ni powder (3-7 μ m)	78	88	91	91
Coarse Ni powder (45-48 μ m)	77	86	92	88

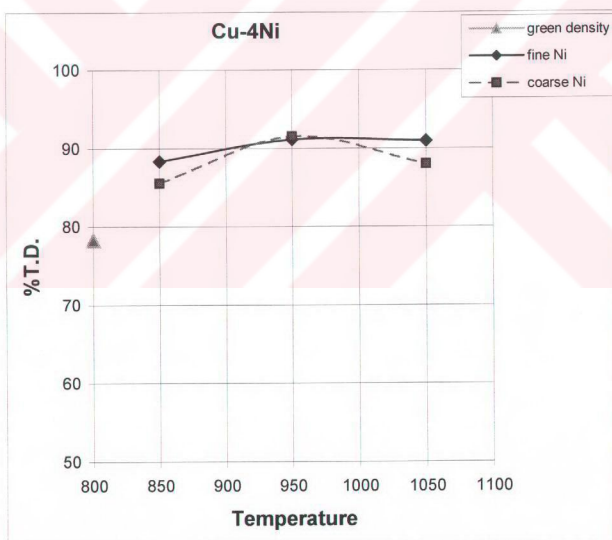


Figure 4.11. The change in density of the cold compacted and sintered Cu-4^w/₀Ni specimens as a function of temperature.

Secondly, sintering studies were carried out on Cu-8^{w/o} Ni powder mixtures in the temperature range 900-1000°C. Change in densities of the specimens with sintering temperature is given in Figure 4.12. The densities of the green compacts with fine Ni powder and coarse Ni powder were very similar around 77-78 %T.D. The density of the compacts increased upon sintering at higher temperatures. For example, 90 %T.D. was obtained upon sintering at 1000°C (Table 4.8).

From the graphs, it can be seen that, for both compositions of the Cu-Ni system, the as-sintered densities were higher than the green densities of the compacts. This is an expected result, since the sintering is in solid state and there is shrinkage after sintering. But, with an increase in sintering temperature, there was not a significant change in final densities of the compacts.

Table 4.8. The change in the density of Cu-8^{w/o} Ni specimens

Cu-8 ^{w/o} Ni	Density before sintering (%T.D.)	%T.D. after sintering at;		
		900°C	1000°C	1100°C
Fine Ni powder (3-7µm)	77	87	92	92
Coarse Ni powder (45-48µm)	76	89	88	92

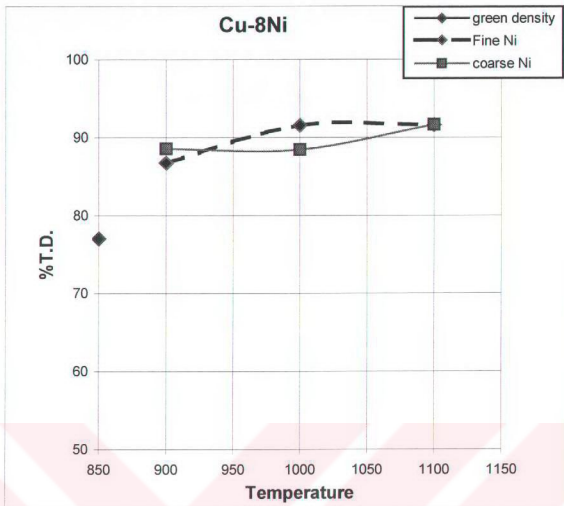


Figure 4.12. Change in density of the cold compacted and sintered Cu-8^w/₀Ni specimens as a function of temperature.

Figures 4.13 and 4.14 are the micrographs of the Cu-Ni specimens compacted at 300 MPa and sintered at different temperatures. The microstructure of the Cu-4^w/₀Ni specimen prepared with fine Ni powder, compacted at 300 MPa and sintered at 950°C for 1 hour can be seen in Figure 4.14. Figure 4.15 is the microstructure of the Cu-8^w/₀Ni specimen prepared with coarse Ni powder, compacted at 300 MPa and sintered at 1100°C for 1 hour. Both microstructures are completely different from the Cu-Al system. Because the Cu-Ni specimens were sintered below their solidus temperatures to obtain solid state sintering. The pores observed in the microstructures are not related to any liquid phase formation. Rather, they are typical for solid state sintering.

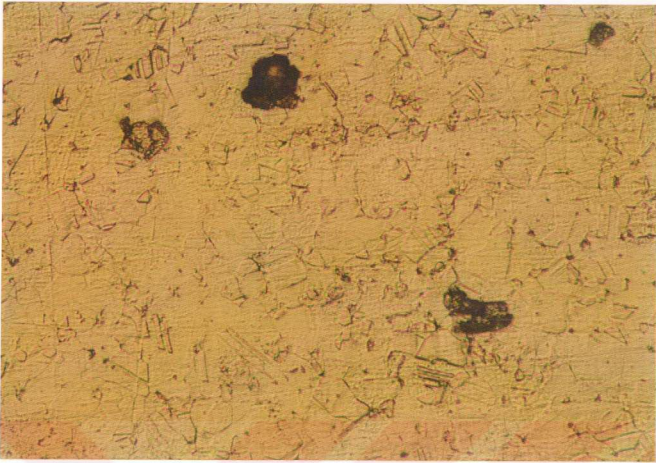


Figure 4.13. The optical micrograph of Cu-4 %Ni, sintered at 950°C

x300

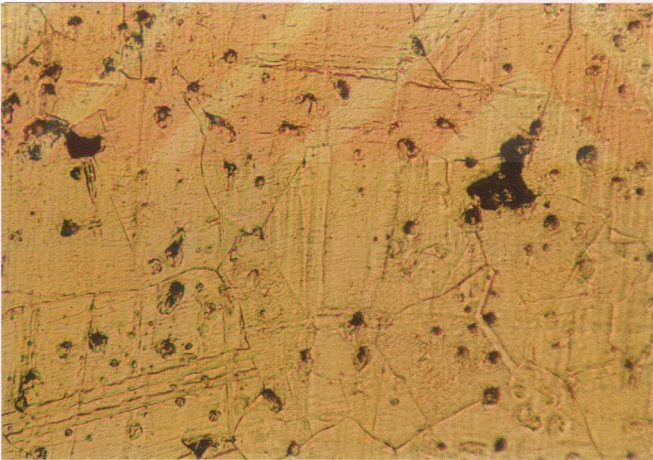


Figure 4.14. The optical micrograph of Cu-8 %Ni, sintered at 1100°C

x300

Under S.E.M., the pores and their locations can be observed clearly (Figure 4.15). As seen, the appearance of the pores in Cu-Ni system is much more different than Cu-Al system. In Cu-Ni system, there isn't any intermetallic phase formation around the pore, which is due to the characteristics of Cu-Ni phase diagram. It is important to note that the Ni powders also leave pores behind during sintering.

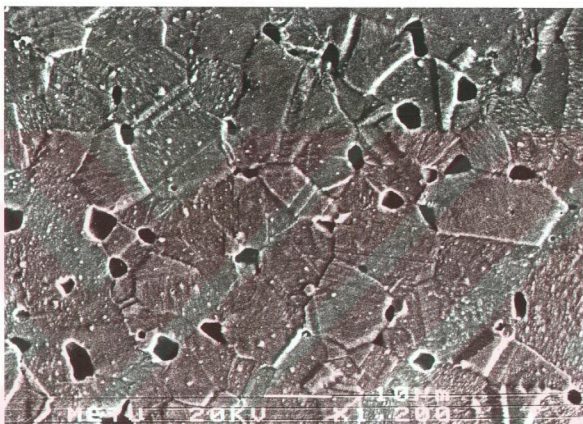


Figure 4.15. The S.E.M. photograph of Cu-4^w/₀Ni, sintered at 950°C x1200

The beneficial effect of compaction pressure on densification, which was previously observed in the Cu-Al compacts, would also be seen in the Cu-Ni compacts. For this purpose, Cu-4^w/₀ Ni specimens, prepared from two different size of Ni powder, were compacted at 700 MPa, and were sintered at three different temperatures. The investigated systems, sintering temperatures and final densities are given in Table 4.9.

Table 4.9. Sintering temperatures and the final densities of the Cu-4^w/₀Ni specimens

Cu-4 ^w / ₀ Ni	Density before sintering (%T.D.)	%T.D Density after sintering at;		
		850°C	950°C	1050°C
Fine Ni powder (5 μm)	89	84	83	83
Coarse Ni powder (46 μm)	89	83	82	82

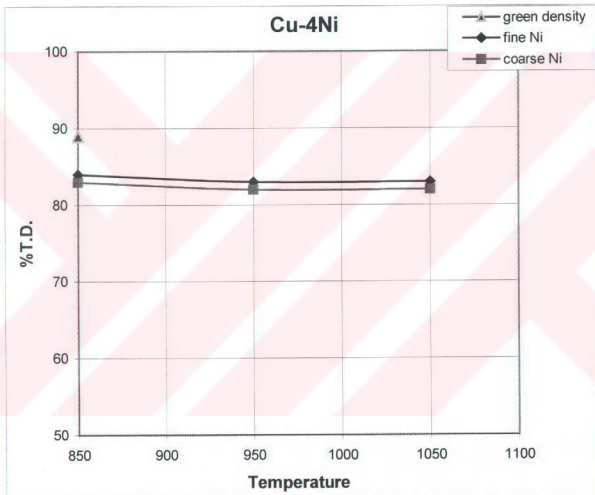


Figure 4.16. Change in density of the Cu-4^w/₀Ni specimens compacted at 700 MPa

As can be seen in Figure 4.16, the Cu-Ni specimens compacted at 700 MPa has very high green densities. But after sintering, in contrast to the specimens compacted at 300 MPa, there is a decrease in densities due to swelling of the compacts.

4.3. SINTERING STUDIES ON Cu-Al-Ni SYSTEM

The above studies on the binary systems showed that, higher compaction pressures yield higher sintered densities after any sintering route. Considering this result, the Cu-Al-Ni specimens compacted at 700 MPa, were sintered by following different routes. The investigated systems, sintering routes and final densities are given in Table 4.10. As seen, sintering at low temperatures cause the swelling of specimen. The density of the specimen sintered at 500 °C for two hours dropped from 78%T.D. to 72%T.D.

Table 4.10. Sintering routes and the densities of the Cu-12 w/o Al-4 w/o Ni specimens compacted at 700 Mpa

Cu-12 w/o Al-4 w/o Ni	500 °C (2 hours)	500 °C (2 hours) + 1000 °C (1 hour)	1000 °C (1 hour)
Density before sintering (%T.D.)	78	78	78
Density after sintering (%T.D.)	72	76	79

In the metallographic examinations of the Cu-12 w/o Al-4 w/o Ni specimens, it was observed that, the structure contains pores like in the Cu-Al system. Figure 4.17 belongs to the Cu-12 w/o Al-4 w/o Ni specimen compacted at 700 MPa and sintered at 1000°C for 1 hour. The phases formed after sintering is different from Cu-Al specimens, but the porosity is very similar to the one observed in Cu-Al system.

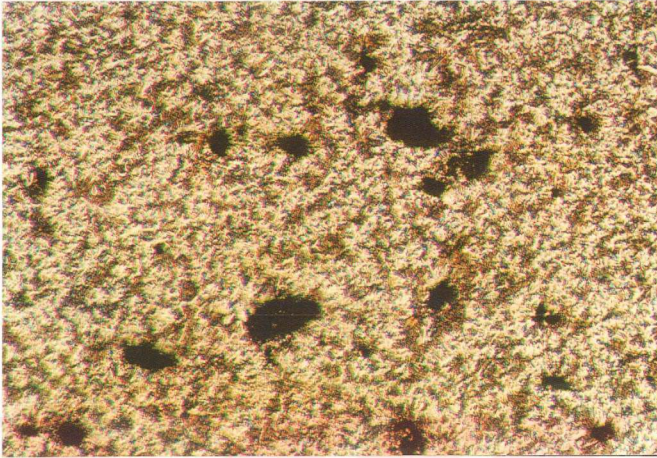
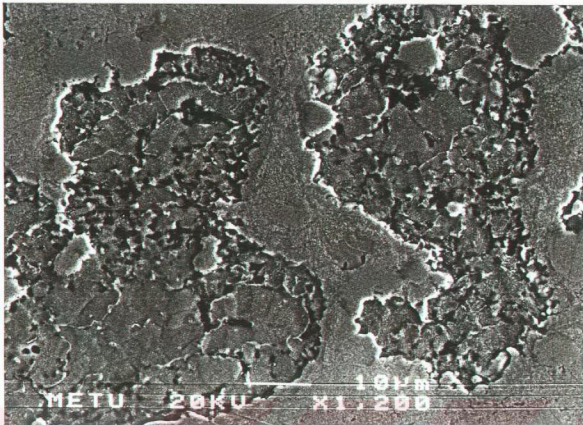


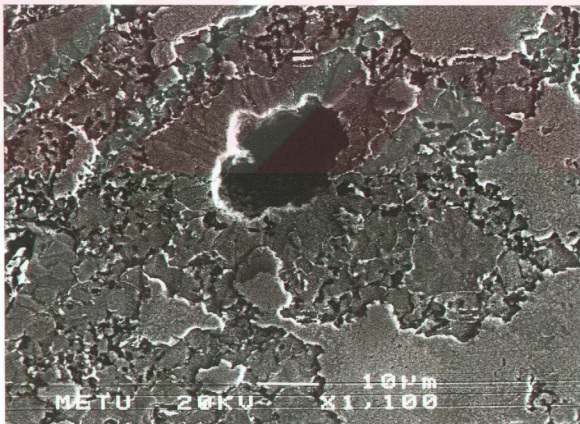
Figure 4.17. The optical micrograph of Cu-12 ^w/₀ Al-4 ^w/₀ Ni, sintered at 1000°C x75

The Cu-12 ^w/₀ Al-4 ^w/₀ Ni specimen compacted at 700 MPa and sintered at 500°C for 2 hours was examined under scanning electron microscopy. The microstructure of this specimen can be seen in Figure 4.18.

In Figure 4.18-b, the Al and Ni powders could be distinguished since, their difference in size (i.e. Al \approx 26 μ m, Ni \approx 5 μ m). An EDS analysis taken from the matrix shows a composition of 82 ^w/₀ Cu-13 ^w/₀ Al-5 ^w/₀ Ni, which is very close to the aimed composition of Cu-12 ^w/₀ Al-4 ^w/₀ Ni. This result shows that, diffusion rate is very fast even at a low temperature (i.e. 500°C) in the ternary system.



a) x1200



b) x1100

Figure 4.18. S.E.M. photograph of Cu-12^{wt%}Al-4^{wt%}Ni, sintered at 500 °C for 2 hours

4.4. HOT ROLLING STUDIES ON Cu-Al, Cu-Ni AND Cu-Al-Ni SYSTEMS

Hot rolling is a very common process applied for the production of P/M parts. Because, besides giving the desired shape to the material, it also helps to reduce the porosity in P/M parts.

Some specimens produced throughout this study were also hot rolled after sintering. The main aim was to reduce the porosity and to observe the deformability of the compacts. All hot rolling operations were carried out at 900°C by giving 15% reduction at each step. The shape of the specimens before and after hot rolling can be seen in Figures 4.19 and 4.20.



Figure 4.19. A cylindrical sintered compact before hot rolling



Figure 4.20. The appearance of a specimen after hot rolling

Hot rolling was firstly applied to the specimens of the S3 Cu-Al system (Table 4.4), which were compacted at different pressures in a range of 300-700 MPa and were sintered at either 950°C or 1000°C. After hot rolling, cracks were observed in all of the specimens. But, the specimens compacted at higher pressures and sintered at higher densities, were more successfully hot rolled. The thickness values of some S3 specimens, before and after hot rolling are given in Table 4.11.

Table 4.11. Thickness of some S5 specimens before and after hot rolling

Cu-12Al	t_i (cm)	t_r (cm)
S3-2	3.0	1.1
S3-4	3.4	0.9
S3-6	3.1	0.8
S3-8	3.5	0.8

From the given thickness values, total reduction in thickness can be calculated. For example, there was a 77% reduction in the thickness of the S3-8 specimen.

All the specimens were examined metallographically after hot rolling operation. Figure 4.21 shows the microstructure of the hot rolled Cu-12^w% Al specimen, compacted at 500 MPa and sintered at 950°C for 1 hour. The thin black lines are the pores, which were previously spherical and are elongated upon hot rolling.



Figure 4.21. The optical micrograph of Cu-12^w% Al, hot rolled after sintering at 950°C X150

As a second attempt, the Cu-4 ^w/_oNi specimens compacted at 700 MPa and sintered in a temperature range of 850-1050°C were hot rolled. All the specimens were successfully hot rolled without any crack formation. For example, the thickness of the specimen prepared with coarse Ni powder and sintered at 950°C was reduced from 3,4 cm to 0,4 cm successfully.

Since Cu-Ni specimens were successfully hot rolled, it was expected that Cu-Al-Ni system could also be hot rolled without severe crack formation. For this purpose, the Cu-Al and the Cu-Al-Ni systems compacted at 700 MPa and sintered by following three different routes (samples of systems S4 and S5), were hot rolled. The investigated systems and the sintering routes are given in Table 4.12.

Table 4.12. Investigated systems and the sintering routes

Sintering route	500 °C (2 hours)	500 °C (2 hours) + 1000 °C (1 hour)	1000 °C (1 hour)
Cu-Al system	S4 -1	S4 - 2	S4 - 3
Cu-Al-Ni system	S5-1	S5-2	S5-3

When the stepwise sintered and hot rolled Cu-Al specimens were observed under optical microscope, the structure showed cracks at the surface regions like all the other hot rolled Cu-Al specimens. In Figure 4.22, which belongs to the hot rolled S4-2 specimen, the defects in the surface region and the surface cracks can be observed clearly.

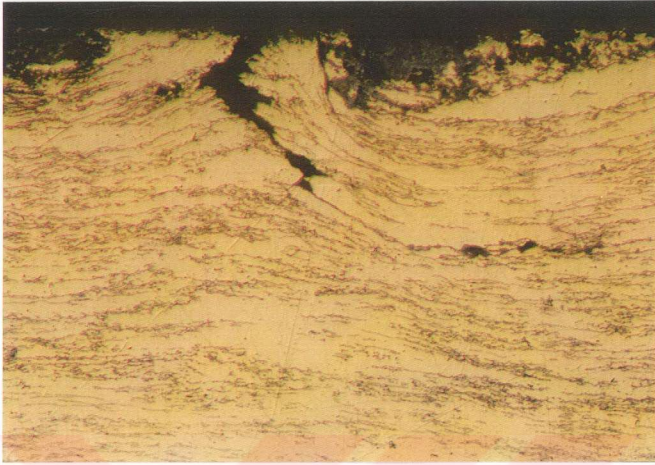
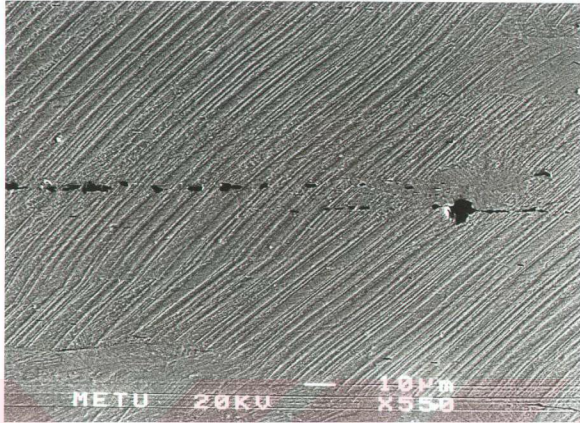


Figure 4.22. Cu-12 %Al, stepwise sintered and hot rolled

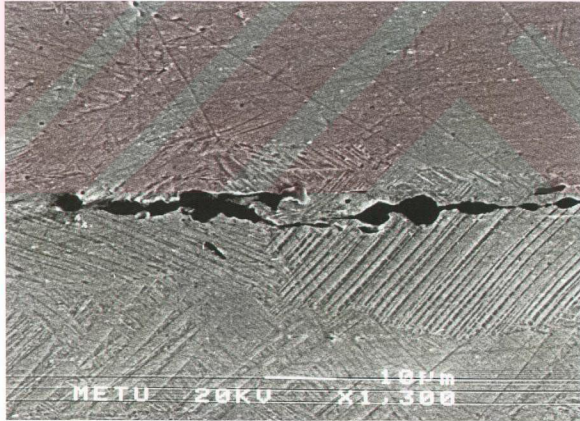
x300

To observe the reason of cracking, the Cu-Al specimens were observed under S.E.M. after hot rolling. Figure 4.23 belongs to the hot rolled Cu-12 %Al specimen compacted at 700 MPa and sintered at 1000 °C for 1 hour (previously denoted as S3-8).

When we look at the microstructures in Figure 4.23, the pores elongated upon sintering (as thin black lines) and the Al₂O₃ inclusions (as black spots) can be clearly identified. The black spots are predicted to be Al₂O₃ inclusions, remained unreduced in the structure. The E.D.S. analysis taken from the black spots also reveals the presence of an oxide inclusion in the structure.



a) x550



b) x1300

Figure 4.23.S.E.M. photograph of Cu-12^w/₀ Al, hot rolled after sintering at 1000°C

The hot rolled Cu-12 % Al-4 % Ni specimen, compacted at 700 MPa and sintered at 1000°C for 1 hour was also observed under S.E.M. As can be seen in Figure 4.24, the structure has partly transformed to martensite and there are again elongated pores in the structure, seen as thin black lines.

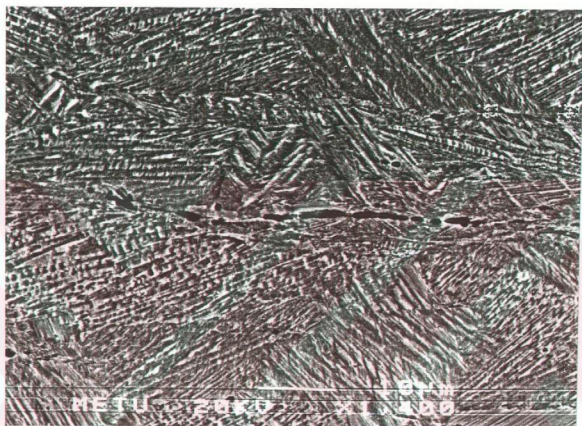


Figure 4.24.S.E.M.photograph of Cu-12 % Al-4 % Ni, hot rolled after sintering at 1000°C x1400

After hot rolling operations, it was observed that neither the Cu-Al nor the Cu-Al-Ni specimens were hot rolled without crack formation. But, crack formation started at the early stages of hot rolling operation in the stepwise sintered specimens, while it started in the later stages of hot rolling operation in the specimens, which were sintered at 1000°C. This result is also supported by the density values attained after sintering. The specimens sintered at 1000°C have higher final densities than the stepwise sintered ones (Table 4.13). The main reason of cracking during hot rolling operation is predicted to be the unreduced Al_2O_3 inclusions. The oxide layer around Al powder and its result in cracking will be discussed in detail in section 5.2.

Table 4.13. Density values of the S4 (Cu-12 %Al) and S5 (Cu-12 %Al-4 %Ni) systems

Specimens	S4-1	S4-2	S4-3	S5-1	S5-2	S5-3
Density before sintering (%T.D.)	78	78	78	78	78	78
Density after sintering (%T.D.)	71	73	79	72	76	79

4.5. GRAIN REFINING STUDIES

Because of rapid grain growth, heat-treated Cu-base shape memory alloys usually possess coarse grains with sizes in the mm range. Coarse-grained Cu-base alloys are brittle and prone to premature intergranular failure. They also exhibit shorter thermomechanical cycling life due to rapid degradation in shape memory performance.

In this study, γ -Al₂O₃ powder is added as a grain-refining element in small amount (0.3 %) and its effect on both the binary and the ternary system is observed. The investigated systems are listed in Table 4.14.

Table 4.14. Compositions and the sintering temperatures of the investigated systems for grain refining studies

Code	Composition (%)				Sintering Temperatures (°C)			
	Cu	Al	Ni	$\gamma\text{Al}_2\text{O}_3$	850	900	950	1000
12Al	88	12	-	-	✓	✓	✓	✓
12Al-0.3G	87.7	12	-	0.3	✓	✓	✓	✓
12Al-4Ni	84	12	4	-	✓	✓	✓	✓
12Al-4Ni-0.3G	83.7	12	4	0.3	✓	✓	✓	✓

The densities were measured before and after sintering, and the obtained densification results are listed in figures 4.25 and 4.26. The attained density values are given in Table 4.15.

Table 4.15. Density values of the investigated systems for grain refining studies.

Code	Density before sintering (% T.D.)	%T.D. after sintering at;			
		850°C	900°C	950°C	1000°C
12Al	70	71	72	75	78
12Al-0.3G	70	69	71	76	79
12Al-4Ni	70	73	73	76	75
12Al-4Ni-0.3G	70	71	72	72	74

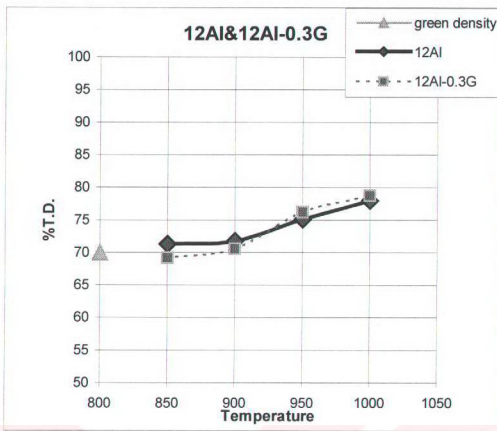


Figure 4.25. Change in density of the cold compacted and sintered Cu-12 %Al specimens as a function of temperature.

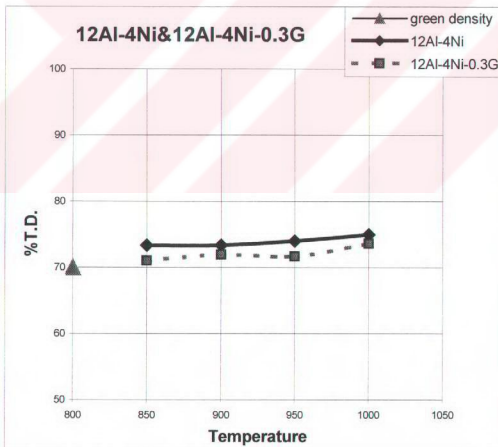


Figure 4.26. Change in density of the cold compacted and sintered Cu-12 %Al-4 %Ni specimens as a function of temperature.

The grain refining effect of $\gamma\text{-Al}_2\text{O}_3$ was investigated in previous studies [48]. As a result, grain size of Cu-Al-Ni system was reduced from 30 μm to 20 μm with $\gamma\text{-Al}_2\text{O}_3$ addition. From the excel graphs of this study, it can be concluded that $\gamma\text{-Al}_2\text{O}_3$ has no significant effect on densification behavior of, both the binary and ternary systems.

CHAPTER 5

DISCUSSION

In recent years shape memory alloys have become popular in the technological world because of their shape memory effect and superelasticity. Among several alloy systems, which reveal shape memory properties [4], only Ti-Ni and Cu-based alloy systems are successfully applied in various industrial projects.

In recent years it is thought that, production of shape memory alloys by powder metallurgical techniques are advantageous, since chemical compositional range can be controlled sensitively and grain growth can be prevented as a result of low process temperatures.

Purpose of this study is to produce Cu-Al-Ni shape memory alloys by conventional powder metallurgical techniques (i.e., cold compaction and sintering) starting from elemental powders. The main aim is to combine the advantages of powder metallurgy with the special properties of shape memory alloys.

5.1. Pore formation in Cu-Al system

In the processing of powder materials, sintering is applied to decrease the porosity and to increase the density. In general, the increase in density depends on the kind of powder materials and the sintering conditions such as temperature and time. However, for a green compact made from mixed composite powders, the density is affected not only by the sintering conditions but also by the combination and volume fraction of the composite powders [50].

As already mentioned in section 4.1, in this study several sintering studies were carried out on the Cu-Al system. In these studies, Cu-Al specimens with several different compositions were compacted at different pressures and were sintered by following different routes. As a result of these processes, Cu-Al specimens showed no densification upon sintering. Compacts with Al content higher than 10^w/_o showed a decrease in density after sintering which can be related to an increase in amount of the pores. Consequently, it can be stated that sintering causes *swelling* of the compact. Swelling can be defined as the increase in compact dimensions, due to pore formation during liquid phase sintering. Only the Cu-12w/oAl specimens compacted at low pressures (300&500 MPa) and sintered at 1000°C showed a small amount of densification upon sintering (Fig. 4.9).

Several studies on the liquid phase sintering of Cu-Al compacts have been made which showed an expansion above the eutectic point temperature of 548°C, and various mechanisms have been suggested [34-36]. German et al. [51] states that there is an important parameter for liquid phase sintering, which is solubility ratio. For a generalized presentation, an additive 'A' will be combined with a base 'B', which can be considered as Cu in our case. Solubility ratio is ' S_B/S_A ', where S_B is the solubility of B in A and, S_A is the solubility of A in B. Swelling is associated with a small solubility ratio, while densification is associated with a large solubility ratio. Additive flow into the base material causes swelling because large pores are formed where additive existed before dissolution.

When we look at the Cu-Al binary phase diagram, it can be seen that, Al has much higher solubility in Cu, than does Cu have in Al. So, their solubility ratio is small and this may lead to the swelling of the compact.

In the other studies it was found that, the flow of the liquid phase produced during heating of Cu-Al powder compacts was important in determining the pore structure and the composition homogeneity [33]. The liquid flow into the capillaries between Cu particles is rapid when wetting is enhanced by reduction of oxide surface films or by increase of Cu concentration in the melt at around 630°C. However, when the green density is very high, the liquid flow is inhibited by the formation of solid phases, probably at the fine capillaries. Lee et al. [33] states that during transient liquid phase sintering, a homogenous composition can readily be obtained, if the flow of the transient liquid into capillaries is rapid. Additionally, pores are produced at the site of the Al particles which form melts, and they can obviously hinder densification.

German et al. [37] states that formation of intermediate compound, which is in solid state during sintering, between the additive and the base will inhibit interdiffusion. This will lead to pore formation and also swelling. On the other hand, Savitskii et al. [34] has related the pore formation to the diffusion of the aluminum particles from the liquid into the solid phase generating voids at the sites of original aluminum particles.

However, in Dericioglu's study, the basic mechanism of pore formation seen in the Cu-Al system is believed to be by the shrinkage of the Al-rich liquid during its solidification as a result of Cu enrichment by diffusion. The solidification in Cu-Al system occurs by an isothermal composition shift during sintering. Pure aluminum regions transform into liquid at the initial stages of sintering, and this liquid solidifies by the rapid diffusion of copper atoms into it during the later stages. As it is a well-known fact that solids are denser than liquids, with a few exceptions,

the solidified regions occupy less space than the liquid does and so pore formation takes place in these regions [48].

Schaffer et al [52] states that the major problem in Cu-Al system is that the diffusivity of copper in aluminum is almost 5000 times faster than that of aluminum in copper. The diffusivity, D , of Cu in Al at 600°C is $5.01 \times 10^{-9} \text{ cm}^2\text{s}^{-1}$ whereas the diffusivity of Al in Cu is $1.14 \times 10^{-12} \text{ cm}^2\text{s}^{-1}$ [53]. While the faster diffusivity of copper in aluminum enhances the rate of homogenization, it causes expansion via the Kirkendall effect. Sintering of the Cu-Al system is therefore dependent on the process variables, particularly the copper particle size and the heating rate [54,55].

In 1947, Ernest Kirkendall reported the results of experiments on the interdiffusion between copper and zinc in brass and observed the movement of the interface between the different phases due to high-temperature interdiffusion, now called the Kirkendall Effect. This phenomenon supported the idea that atomic diffusion occurs through vacancy exchange. Since its discovery, the Kirkendall Effect has been found in various alloy systems, and studies on lattice defects and diffusion developed significantly. The Kirkendall Effect is important in connection with bonding between different materials and, in particular, raises the practical concern of controlling and suppressing the voids that are produced in the boundary region at a bonding interface. Today, the effect has been taken into account in various fields in materials science and technology such as structural materials welding, metals and ceramics powders sintering, thin films, and large-scale integration.

Kirkendall effect, which is caused by the differences in the mutual diffusivities of the constituents, may also contribute to pore formation [34-36]. In order to investigate the Kirkendall effect in the Cu-Al system, solid-state sintering studies were carried out as described in section 4.1. When the micrographs of the specimens sintered at 500 °C are observed (Figures 4.6 & 4.7), it can be seen that, the structure contains pores at the original Al powder sites. Depending on the

sintering time, different phases form around the pore. This result reveals that, the reasons for the formation of pores are not only related to formation of liquid Al, as discussed above. Kirkendall effect can be another factor causing pore formation and swelling. Because, at 500 °C, there is no liquid formation in Cu-Al phase diagram, but we still observe pores.

However, if the main mechanism causing pore formation during solid state sintering was Kirkendall effect, we should have observed the pores not at the original Al powder sites, but at the original Cu powder sites. Because as mentioned before, Cu has 5000 times faster diffusivity in Al, than Al has in Cu. This would cause the formation of a pore at the original Cu powder site.

Additionally, the observed pores are in a few micron size. If the vacancies formed during Kirkendall effect have coalesced and have formed the pores, these pores would be so small that they would not be observed under optical microscope. For example, for the formation of a 1 μm size pore, $\approx 10^8$ vacancies should have coalesced. However, at 500°C, besides vacancy formation, there is also vacancy annihilation, which makes the coalescence of 10^8 vacancies nearly impossible.

5.2. Hot Rolling Studies

In the hot rolling studies, both the binary systems and the ternary system were investigated. The investigated systems and the sintering routes were previously described in section 4.4.

The hot rolling operation on the Cu-Ni specimens was successful. Before hot rolling, pores were observed in their microstructure. However, their thickness could be reduced from 3.4 cm to 0.4 cm without any crack formation. When the microstructures were observed after hot rolling, it was seen that the pores were closed and welded with the help of pressure and heat. Additionally, the CuO_2 and NiO inclusions that are possibly present in the structure have high H_2 reduction

capability. They are easily reduced under H_2 atmosphere and as a result, do not cause crack formation during hot rolling.

In the hot rolled Cu-Al specimens, cracks were observed on the surface and in the regions close to the surface. As can be seen in the micrographs of the hot rolled Cu-Al specimen (Figure 4.23), besides the closed pores upon hot rolling; several inclusions were present in the structure. Analysis taken from these inclusions showed that, these were Al_2O_3 particles. This Al_2O_3 comes from the thin Al_2O_3 film around the Al powder.

Most of the defects observed in the microstructures were in the form of fine cracks, which most probably stem from the closed pores. It seems that these residual pores that originate from the Al powder that could not be closed and welded during hot rolling.

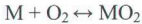
In several other parts of the hot rolled specimens, Al_2O_3 particles, oriented in the direction of rolling, were also observed. These Al_2O_3 particles can belong to the residues left from oxidized Al as mentioned before. Although all sintering processes were carried out in H_2 atmosphere, it is a well-known fact that Al_2O_3 cannot be reduced like Cu-oxide or Ni-oxide. Since oxidation is more favorable on the surface and in the regions close to the surface, most of the cracks and defects are seen in these regions (Figures 4.22).

Aluminum is always covered by an oxide. The thickness of the oxide is dependent on the temperature at which it is formed and the atmosphere in which it is stored, particularly, the humidity [52]. The oxide crystallizes to γ - Al_2O_3 on prolonged annealing at temperatures above 350 °C [56-58]. The oxide prevents solid state sintering in low melting point metals. This has been explained in terms of the relative diffusion rates through the oxide and the metal, for metals with stable oxides. The use of liquid phases is an alternative to solid state sintering. As an essential requirement for effective liquid phase sintering is wetting of the liquid

phase. High melting point metal oxides are generally purely wetted by liquid metals [52].

It has been suggested that the Al-CuAl₂ eutectic can wet Al₂O₃ at 600 °C. However, neither Mg, Ce nor Ca additions to molten Al increase the wettability [60,61]. It is therefore apparent that the oxide on aluminum is a barrier to sintering and needs to be disrupted or otherwise removed.

The oxidation of a metal, M, may be represented as;



The free energy of formation, ΔG , of the oxide is given by

$$\Delta G = -RT \ln K_1$$

Where R is the gas constant, T the temperature in Kelvin and K₁ the equilibrium constant given by;

$$K_1 = (P_{O_2})^{-1}$$

Where P_{O₂} is the partial pressure of oxygen.

For aluminum at 600 °C, a P_{O₂} < 10⁻⁵⁰ atm is required to reduce the oxide [55]. Atmospheres containing hydrogen are often used in powder metallurgy. Hydrogen can reduce a metal oxide by the reaction:



The equilibrium constant for this reaction, K₅ is given by,

$$K_5 = P_{H_2O} / P_{H_2}$$

Where P_{H₂} and P_{H₂O} are the partial pressure of hydrogen and water vapor, respectively. The ratio of the partial pressures can be converted to dew point, effectively the water vapor content. A dew point of ≤ -140 °C at 600 °C is required to reduce Al₂O₃ [56]. Neither a dew point of -140 °C nor a P_{O₂} of 10⁻⁵⁰ is

physically attainable and therefore aluminum cannot be sintered in conventional atmospheres [52].

In conclusion, The Al_2O_3 originated from Al powder or as an oxidation product can stay as a residue in the structure and form Al_2O_3 inclusions.

The ternary system Cu-Al-Ni specimens were also hot rolled. Their composition was Cu-12 w/o Al-4 w/o Ni and they were compacted at 700 MPa. The hot rolling temperature was determined as 900°C. Similar to Cu-Al specimens, cracks were observed in the hot rolled Cu-Al-Ni specimens. The reason is the same with Cu-Al specimens, which is the unreduced Al_2O_3 particles in the structure. It can be also seen in the micrographs of the hot rolled Cu-Al-Ni specimens (Figure 4.24). There are thin black lines, which are the closed pores upon sintering, and black spherical inclusions. These spherical inclusions are the Al_2O_3 particles, since Al_2O_3 is a hard phase, its shape does not change much with hot rolling. Compositional analyses taken from these inclusions also support this idea, and show that they are oxide particles, which originate from the Al powder.

The result of the EDS analysis taken from the hot rolled Cu-Al-Ni specimens compacted at 700 MPa and sintered at 1000°C, showed 82.45 % Cu, 13.3 % Al and 4.25 % Ni, which is very close to the aimed composition for the ternary system. As a result, it can be concluded that, homogenization is almost completed throughout the specimen.

5.3. Effect of Compaction Pressure and Sintering Route on the Final Density

It is already known that, compaction pressure has significant effects on the densification and final density of green compacts.

In this study, the Cu-Ni specimens were compacted at 300 & 700 MPa and were sintered in a temperature range of 850-1050°C. The specimens compacted at 300

MPa had green densities around 78 %T.D. After sintering their densities were increased to around 90 %T.D. however, the specimens compacted at 700 MPa had green densities around 89 %T.D and their density was slightly reduced to 83 %T.D after sintering (Figure 4.16).

Moreover, the Cu-12 % Al specimens were compacted in a pressure range of 300-700 MPa and were sintered at either 950 or 1000°C (Table 4.4). It can be concluded from Figure 4.9 that, as the compaction pressure increases, densification after sintering at 950 or 1000 °C shows a decrease. For example, the specimen compacted at 300 MPa have a final density of 71 %T.D. after sintering at 950°C, and a final density of 76 %T.D. after sintering at 1000°C. However, the specimen compacted at 700 MPa have same final densities after sintering either at 950 °C or 1000°C.

This result is in accordance with R.German. German states that, high pressures increase density by contact enlargement through plastic deformation. Thus, the pressure causes localized deformation at the contacts, giving work hardening and allowing new contacts to form as distance between particles decreases. As the compaction pressure is further increased, the amount of each particle undergoing plastic deformation increases. With sufficient pressurization, the entire particle becomes work hardened as the amount of porosity decreases. Consequently, any further gains in the green density require even greater expenditures of energy from the external pressure source [31].

At high compaction pressures, because of the lower porosity, there is less shrinkage during sintering. The higher dislocation density contributes to an initially faster sintering rate. Compaction therefore contributes to increased strength, density, shape definition and dimensional control. The higher compaction pressures contribute to an increase in density and neck contact size, while reducing the rate of neck growth during sintering. Also, shrinkage decreases with an increase in compaction pressure.

Another important factor affecting the final density is the sintering route. The most obvious effect is observed in the Cu-Al and Cu-Al-Ni specimens compacted at 700 MPa pressure and sintered by following three different routes.

Figure 5.1 shows the final densities for the Cu-12 w/o Al binary, and Cu-12 w/o Al-4 w/o Ni ternary systems, after different sintering routes. The sintering **route A** designates sintering at 500°C for 2 hours, sintering **route B** designates sintering at 500°C for 2 hours and then sintering at 1000°C for 1 hour, sintering **route C** designates sintering at 1000°C for 1 hour.

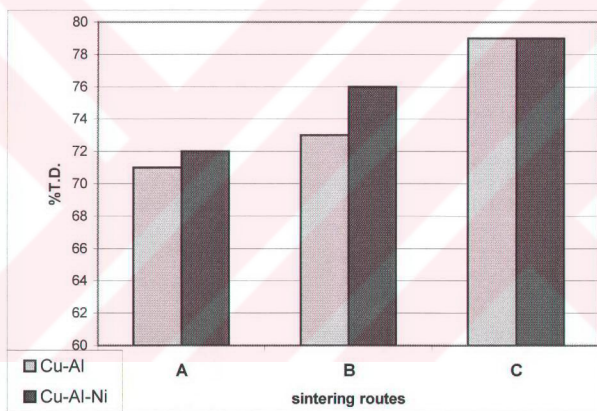


Figure 5.1. Change in densities of the investigated Cu-Al and Cu-Al-Ni systems after sintering routes A, B, and C.

(**Route A:** sintering at 500 °C for 2 hours; **Route B:** sintering at 500°C for 2 hours and then sintering at 1000°C for 1 hour; **Route C:** sintering at 1000°C for 1 hour)

It is seen that, there is a large difference in the final densities obtained after route B and route C for both alloy systems. Since the main difference between the two routes is the presence of solid state sintering, the reason of the densification difference should be related to some mechanism that is taking place during solid-state sintering. As mentioned before, Cu has 5000 times higher diffusivity than Al has. It was previously stated by Lumley et al. [54,55] that, while the faster diffusivity of Cu in Al enhances the rate of homogenization, it causes expansion via the Kirkendall effect. So, once there is an expansion in the specimen during solid state sintering, the increased sintering temperature and liquid phase sintering cannot contribute much to densification. As a conclusion, this may result in a lower final density than the specimen sintered by following route C.

CHAPTER 6

CONCLUSION

As a result of the current study about production of Cu-Al-Ni shape memory alloys by Powder Metallurgical techniques, the following can be stated as conclusion.

1. During the sintering studies on Cu-Al system, pore formation in the powder compacts could not be prevented. However, as a result of solid state sintering studies, it was observed that, the compositional solidification of a liquid phase is not the only reason of pore formation.
2. The Cu-Al and Cu-Al-Ni powder compacts could not be hot rolled without crack formation. The Al_2O_3 inclusions originating from Al powder caused cracking on the surface. Therefore, the shape memory behavior of the Cu-Al-Ni samples could not be investigated due to the cracks observed after hot rolling.

3. Cu-Ni powder mixtures were successfully hot rolled after sintering. The small amount of porosity observed after sintering was almost eliminated. Because, the present pores were closed and welded during hot rolling with the help of pressure and temperature.

4. The main reason of cracking during hot rolling was found to be Al_2O_3 inclusions. These inclusions originated from the Al powder and could not be reduced under H_2 atmosphere. Because, the required dew point and O_2 pressure values to reduce Al_2O_3 were not physically attainable in conventional atmospheres.

REFERENCES

- [1] L.C. Chang and T.A. Read, Trans. AIME, 189 (1951), pp47
- [2] R.D.Jean, T.Y.Wu and S.S.Leu, Scripta Metall. Et Mat., Vol.25, pp 883, 1991
- [3] K.Otsuka and C.M. Wayman, Shape Memory Materials, 1998
- [4] TW Duerig, KN Melton, D Stöckel, CM Wayman; Engineering Aspects of Shape Memory Alloys, 1990
- [5] L.Lu, M.O.Lai, and S. Zhang, Materials Sci. and Tech., 10, 319, 1994
- [6] R.D.Jean, T.Y.Wu and S.S.Leu, Scripta Metall. Et Mat., 25, 883, 1991
- [7] S.M. Tang, C.Y. Chung and W.G. Liu, J. of Materials Processing Tech. 63, 1997, pp 307-312
- [8] T.W. Duerig, J. Albrecht And G.H. Gessinger, J. of Metals, 1982
- [9] Darel E. Hodgson, Shape Memory Applications, Inc., Ming H. Wu, Memory Technologies, and Robert J. Biermann, Harrison Alloys, Inc.
- [10] Hiroyasu Funakubo, Shape Memory Alloys,
- [11] John D. Verhoven, Fundamentals of Physical Metallurgy.
- [12] K. Shimizu and T. Tadaki, Shape Memory Alloys, edited by H. Funokubo, Gordon and Breach Science Publishers, 1984
- [13] T.Tadaki, K. Otsuka, K.Schimizu, Ann. Rev. Materials Sci.
- [14] L. Delaey, Van Humbeeck, N. Mwamba, Metals Forum, 1981, 4
- [15] K.Otsuka and K. Schimizu, Scripta Metall., 1970,4

- [16] N. Mwamba and L. Delaey, Proc. Of Int. Conf. On Martensitic Transformations, 1982
- [17] J.M. Guilemany and F.J. Gil, Materials Letters, 1990,10
- [18] M.H. Wu, S.L. Semiatin and L.M. Schecky, Materials Char., 1994, 32
- [19] S. Eucken, Progress in Shape Memory Alloys
- [20] Jansen, J. ,Willems, F. Verelst, B. ,MaertensProceedings, Int. Conf. On Martensitic Transformations, 1982
- [21] Miyazaki, S., Otsuka, K., Sakamoto, H. and Shimizu, K. Trans. Jap. Inst. Of Metals,4
- [22] Eucken, S. and Hongobogen, E., Proceedings, Int. Conf. On Martensitic Transformations, 1986
- [23] Stobbs, W.M. and Wood, J.V. Acta Met. , 1979
- [24] Perkins, J. Raymant, J.J. and Cantor, B., Proceedings, Int. Conf. On Solid to Solid Phase Transformations
- [25] R.M. German, Powder Metallurgy Science,
- [26] Joel S. Hirschhorn, Introduction To Powder Metallurgy
- [27] R.L. Sands and C.R. Shakespeare, Powder Metallurgy Practice and Applications, William and Clowes and Sons Ltd., London, 1996, pp 78
- [28] Lenel, F.V. Powder Metallurgy, Metal Powder Industries Federation, 1980
- [29] Metals Handbook, Volume 8, American Society for Metals
- [30] Exner, H.E. Principles of Single Phase Sintering, 1979
- [31] R.M. German, Sintering Theory and Practice, 1996
- [32] R.M. German, Liquid Phase Sintering, 1985
- [33] Doh-Jae Lee and Duk N. Yoon, Powder Met. Int., vol.20, no.5, 1988
- [34] K.V. Savitskii, V.I. Itin, Yu. I. Kozlov, A.P.Savitskii, Soviet Powder Met. Metal Ceram. 4, 1965, pp 886

- [35] K.V. Savitskii, V.I. Itin, Yu. I. Kozlov, Soviet Powder Met. Metal Ceram. 5, 1966, pp 4
- [36] A.P. Savitskii, M.A. Emelyanova, N.N. Brutsev, Soviet Powder Met. Metal Ceram. 21, 1982, pp 375
- [37] R.M. German, J. of Metals, 1986
- [38] S.-J.L. Kang, W.A. Kayseer, G. Petzow, D.N. Yoon, Powder Metallurgy, 27 (1984), pp 97
- [39] W.A. Kayseer, G. Petzow, Powder Metallurgy, 28, (1985), pp 473
- [40] W.A. Kayseer, S.Takajo, G. Petzow, Modern Dev. In Powder Met., 12 (1981), pp 473
- [41] W.A. Kayseer, G. Schneider, G. Petzow, Prakt. Metallographic 21, (1984), pp13
- [42] K. Tabeshfar, G.A. Chadwick, Proc. Int. P/M Conf., 1982, pp 693
- [43] K. Tabeshfar, G.A. Chadwick, Powder metallurgy, 27 (1984), pp 19
- [44] N. Ddautzenberg, H.J. Dorweiler, Powder Metall. Int. 17 (1985), pp 279
- [45] H. Danniger, Powder Met. Int., vol.20, no.1, 1988
- [46] B.H. Alexander and R.W. Balluffi, Acta Metal, 1957
- [47] C.Y.Chung and C.W.H. Lam, Materials Science and Eng.A273-275, 1999, pp 622-624
- [48] A. Dericioğlu, Master Thesis in Met. & Mat. Engineering, METU, Ankara, TURKEY, 1999
- [49] F.C. Gürhan, Master Thesis in Met. & Mat. Engineering, METU, Ankara, TURKEY, 2001
- [50] K. Yamaguchi, N. Takakura and S. Imatani, J. of Mater. Processing Tech., 63, (1997), pp 364
- [51] R.M. German and B.H. Rabin, Powder Metallurgy, 1985 Vol.28, pp 7
- [52] G.B. Schaffer, T.B. Sercombe and R.N. Lumley, Mater. Chemistry and Physics, 67, (2001), pp 85

- [53] H. Mehrer, Landolt Bornstein Numerical Data and Functional Relationships in Science and Technology, Vol 3/26, 1991
- [54] R.Lumley and G.B. Schafer, Scripta Mater. 35, (1996), pp 589
- [55] R.Lumley and G.B. Schafer, Scripta Mater. 39, (1998), pp 1089
- [56] M.H. Jacobs, J. Microsc. 99, (1972), pp 165
- [57] K. Shinohara, T.Seo, H. Kyogoku, Zeitschrift fur Metallkunde 73, (1982), pp 774
- [58] H.J. van Beek, E.J. Mittemeijer, Thin Solid Films 122, (1984), pp 131
- [59] R.F. Smart, E.C. Ellwood, Nature 181, (1958), pp 833
- [60] S.W. Ip, M. Kucharski, J.M. Toguri, J. Mater. Sci. Lett. 12, (1993), pp 1699
- [61] Y. Liu, Z. He, G. Dong, Q. Li, J. Mater. Sci. Lett., 11, (1992), pp 896